eNeuro

Research Article: Failure to Replicate | Sensory and Motor Systems

Levels of Cocaine and Amphetamine-Regulated Transcript in Vagal afferents in the mouse are unaltered in response to metabolic challenges

CART in the mouse vagal sensory neurons

Xuefeng Yuan[1,2], Ying Huang[1], Sarita Shah[1], Hua Wu[2] and Laurent Gautron[1]

[1]*Division of Hypothalamic Research and Department of Internal Medicine, The University of Texas Southwestern Medical Center, 5323 Harry Hines Blvd., Dallas, Texas 75390*

[2]*Department of Orthopedics, Tongji Hospital, Tongji Medical College, Huazhong University of Science and Technology, Wuhan, China*

DOI: 10.1523/ENEURO.0174-16.2016

Received: 22 June 2016

Revised: 15 September 2016

Accepted: 16 September 2016

Published: 22 September 2016

Author Contributions: XY, YH, and SS performed research; HW provided student; LG performed research, analyzed data and wrote the paper.

Funding: American Neurogastroenterology and Motility Society
research grant 2013-2014

Funding: National Center for Advancing Translational Sciences of the NIH
UL1TR001105

The authors declare no competing financial interests

This work was supported by the American Neurogastroenterology and Motility Society Research Grant (2013-2014). The research reported in this publication was also supported by the National Center for Advancing Translational Sciences of the National Institutes of Health under award #UL1TR001105.

Correspondence should be addressed to Laurent Gautron, 5323 Harry Hines, E-mail: Laurent.Gautron@UTSouthwestern.edu

Cite as: eNeuro 2016; 10.1523/ENEURO.0174-16.2016

1. Levels of Cocaine and Amphetamine-Regulated Transcript in Vagal afferents in the mouse are unaltered in response to metabolic challenges

2. Anatomical characterization of CART in vagal sensory neurons

3. Authors: Xuefeng Yuan[1, 2,] Ying Huang[1], Sarita Shah[1], Hua Wu[2], Laurent Gautron[1]

Affiliations:

[1]Division of Hypothalamic Research and Department of Internal Medicine, The University of Texas Southwestern Medical Center, 5323 Harry Hines Blvd., Dallas, Texas 75390.

[2]Department of Orthopedics, Tongji Hospital, Tongji Medical College, Huazhong University of Science and Technology, Wuhan, China

4. XY, YH, and SS performed research; HW provided student; LG performed research, analyzed data and wrote the paper.

5. Correspondence should be addressed to (include email address):

Laurent Gautron,

5323 Harry Hines Laurent.Gautron@UTSouthwestern.edu

6. Number of Figures: 12 figures; 2 tables; 1 video file.

7. Number of words for Abstract: 212; Number of words for Significance Statement: 101; Number of words for Introduction: 608; Number of words for Discussion: 1,189.

8. Acknowledgements: We are grateful to the members of the UT Southwestern Live Cell Core Facility. We thank Dr. John Wood (University College London) for providing us $Na_v1.8$-Cre mice. We thank Dr. William Holland and Trevor Tippetts (both at UTSouthwestern Touchstone Diabetes Center) for giving us rats. We thank Dr. Pierre-Yves Risold (Université de Franche-Comté) for his input on the murine MCH system. We are also grateful to Solène and Syann Lee for editing our cover letter.

9. Conflict of Interest.

A. The authors declare no competing financial interests

10. Funding sources: This work was supported by the American Neurogastroenterology and Motility Society Research Grant (2013-2014). The research reported in this publication was also supported by the National Center for Advancing Translational Sciences of the National Institutes of Health under award #UL1TR001105.

Levels of Cocaine and Amphetamine-Regulated Transcript in Vagal afferents in the mouse are unaltered in response to metabolic challenges

Running title: Feeding-dependent regulation of the neuropeptidergic profile of the mouse vagal sensory neurons

Abstract

Cocaine and Amphetamine-regulated Transcript (CART) is one of the most abundant neuropeptides in vagal afferents, including those involved in regulating feeding. Recent observations indicate that metabolic challenges dramatically alter the neuropeptidergic profile of CART-producing vagal afferents. Here, using confocal microscopy, we re-assessed the distribution and regulation of CART (55-102) immunoreactivity in vagal afferents of the male mouse in response to metabolic challenges, including fasting, high-fat diet feeding. Importantly, the perikarya and axons of vagal C-fibers were labeled using mice expressing channelrodhopsin-2 (ChR2-YFP) in $Na_v1.8$-Cre-expressing neurons. In these mice, approximately 82% of the nodose ganglion neurons were labeled with ChR2-YFP. Furthermore, ChR2-YFP-labeled axons could easily be identified in the dorsovagal complex. CART (55-102) immunoreactivity was observed in 55% of the ChR2-YFP-labeled neurons in the nodose ganglion and 22% of the ChR2-YFP-labeled varicosities within the area postrema of fed, fasted and obese mice. The distribution of positive profiles was also identical across the full range of CART staining in fed, fasted and obese mice. In contrast to previous studies, fasting did not induce melanin-concentrating hormone immunoreactivity in vagal afferents. Moreover, prepro-MCH mRNA was undetectable in the nodose ganglion of fasted mice. In summary, this study showed that the perikarya and central terminals of vagal afferents are invariably enriched in CART and devoid of MCH.

Significance statement

Recent studies reported that fasting triggers vagal afferents to switch from expressing anorectic to orexigenic neuropeptides. This study failed to replicate the aforementioned observations using a combination of confocal microscopy, immunohistochemistry, and in situ hybridization. In particular, we showed that neither fasting nor diet-induced obesity influence the immunoreactivity for Cocaine and Amphetamine-regulated Transcript neuropeptide in the mouse vagal afferents. In contrast to previous studies, we also failed to detect melanin-concentrating hormone expression in the mouse vagal afferents. Overall, we reached the conclusion that the neuropeptidergic profile of the vagal afferents involved in feeding is remarkably stable in response to metabolic challenges.

Introduction

Over 16 years ago, Broberger and colleagues (Broberger et al., 1999) showed that Cocaine and Amphetamine-regulated Transcript (CART) was expressed in half of vagal afferents, making it one of the most abundantly expressed neuropeptides in the nodose ganglion. Different CART peptides can be generated by splicing and enzymatic cleavage of a precursor peptide in a tissue-specific manner (Koylu et al., 1997; Thim et al., 1999). The long form of CART is highly expressed in the hypothalamus and is considered to be one of the most biologically active CART peptides with proven anorectic actions (Stanley et al., 2001). In the past, CART expression in the nodose ganglion was mainly detected using antibodies raised against the long form of CART (Broberger et al., 1999; Zheng et al., 2002).

Recent pharmacological and RNA interference experiments suggested that vagally-released CART was implicated in the anorectic actions of cholecystokinin (CCK) (De Lartigue et al., 2010; Heldsinger et al., 2012). Most CART-containing vagal afferents were shown to co-express CCK receptor (Broberger et al., 1999), further ascertaining the role of vagally-released CART in feeding. In addition, one retrograde tracing study showed that many CART-positive vagal afferents project to the rat duodenum and stomach (Zheng et al., 2002). Inconsistent observations have also been reported regarding the anorectic actions of CART in the brain (Rogge et al., 2008). In particular, administration of CART in the 4th ventricle suppressed feeding (Aja et al., 2002), CART microinjection into areas of the nucleus of the solitary tract supplied by CART-positive afferents was ineffective at suppressing feeding (Zheng et al., 2002). Hence, the role of vagally-released CART in feeding is controversial. In addition, CART regulation in vagal afferents in response to metabolic challenges remains confusing. One initial study reported that the percentage of rat nodose ganglion cells expressing CART mRNA remains unchanged after food restriction or diet-induced obesity (Broberger et al., 1999). Arguing against these results, several studies reported profound alterations in the neuropeptidergic profile of CART-positive afferents upon fasting. Specifically, fasting and leptin receptor deficiency in vagal neurons were shown to suppress CART immunoreactivity in the rat and mouse nodose ganglia (de Lartigue et al., 2007; De Lartigue et al., 2010; de Lartigue et al., 2014; de La Serre et al., 2015). Furthermore, the orexigenic peptide melanin-concentrating hormone (MCH) was shown to be induced in the vagal afferents of fasted rats and mice that expressed CART in the fed condition (Burdyga et al., 2006; de Lartigue et al., 2007; de Lartigue et al., 2014; de La Serre et al., 2015). To our knowledge, such a unique feeding-dependent switch in the neuropeptidergic profile of vagal afferents had never been reported before.

Given the aforementioned discrepancies and gaps in the literature, the first goal of this study was to re-examine CART (55-102) immunoreactivity in the cell body and axons of vagal C-fibers in mice submitted to different metabolic challenges. We utilized transgenic mice in which $Na_v1.8$-expressing neurons are labeled with channelrhodopsin-2 (ChR2) fused with yellow fluorescent protein (YFP) ($Na_v1.8$-Cre-ChR2-YFP mice) to identify vagal C-fibers. The second goal of this study was to characterize $Na_v1.8$-Cre-ChR2-YFP mice as a useful model to label vagal C-fibers. $Na_v1.8$-expressing peripheral afferents include all of the C-type peripheral afferents, as well as those expressing neuropeptides (Chiu et al., 2014; Usoskin et al., 2015). ChR2-YFP was chosen as a fluorescent reporter due to the emerging evidence of its usefulness in neuronal tract tracing studies (Jennings and Stuber, 2014). Unexpectedly, the present study showed that CART (55-102) present in the perikarya and central terminal of the vagal C-fibers was not regulated by metabolic challenges. In contrast to previous studies, we showed that CART-positive afferents in the mouse never produced MCH.

Materials and methods

Generation of animals and the experimental groups

$Na_v1.8$-Cre-ChR2-YFP mice were generated by crossing $Na_v1.8$-Cre mice (Scn10atm2(cre)Jnw), which were kindly provided to us by Dr. Wood (Stirling et al., 2005), with Ai32 mice (Ai32(RCL-ChR2(H134R)/EYFP) expressing ChR2-YFP in a Cre-dependent manner. The Ai32 mice were originally designed by the Allen Institute (Madisen et al., 2010) and are currently available from the Jackson Laboratory (stock No 012569). The mice were all adult males (ages varying between 6 and 16 weeks of age) carrying one copy of $Na_v1.8$-Cre- and one copy of ChR2-YFP. $Na_v1.8$-Cre mice are useful for selectively inducing the expression of fluorescent proteins in C-fiber neurons, including those in the vagus nerve. The usefulness of Ai32 mice in optogenetic and tracing experiments is also well-documented (Daou et al., 2013; Munoz et al., 2014).

The experimental animals were housed in a barrier facility in a temperature-controlled environment (lights on: 06:00–18:00) with *ad libitum* access to water and standard chow with 12% of calories from fat. All animal procedures were performed in accordance with the guidelines of our Institutional Animal Care and Use Committee at UTSouthwestern Medical Center. For the metabolic challenges studies, we used a total of 22 $Na_v1.8$-Cre-ChR2-YFP mice, which were divided into three groups consisting of animals fed chow *ad libitum* at all times (24.7 ± 0.9 grams body weight, n=7), animals fasted between 16 and 24 hours before sacrifice (21.8 ± 1.2 grams body weight, n=7), and animals fed a high-fat diet (62% calories from fat; Research Diet D12492i) for 4 weeks before sacrifice (35.0 ± 2.4 grams body weight, n=8). A separate group of $Na_v1.8$-Cre-ChR2-YFP mice that were fed on chow *ad libitum* was used for the initial characterization of ChR2-YFP expression in the nodose ganglia and brains (n=4). Another group of 4 $Na_v1.8$-Cre-ChR2-YFP mice was used to map the peripheral organs.

A total of 8 C56/Bl6 male mice (6 weeks of age) divided into fed and fasted groups were also used for performing *in situ* hybridization. These mice were purchased from our institution animal husbandry and housed in the same barrier facility and environment as the $Na_v1.8$-Cre-ChR2-YFP mice. Immunostaining was also performed in the nodose ganglia of six Lean Zucker male rats (6 months of age) that were given to us by another laboratory on our campus. Rats were housed in a conventional facility in a temperature-controlled environment with *ad libitum* access to water and standard chow. Three rats were fed chow *ad libitum* at all times and three were fasted 16 hours before sacrifice.

Tissue collection and preparation for immunohistochemistry

On the day of sacrifice, between 9 and 11 A.M., the animals received an overdose of chloral hydrate (500 mg/kg, i.p.) and were then perfused transcardially with 0.9% saline followed by 10% formalin (Sigma) for 2 minutes. Tissues, including the left nodose ganglion, were rapidly removed with the help of a dissecting scope and post-fixed for approximately 1 hour. The nodose ganglion, brain, stomach wall and duodenum were submerged in 20% sucrose overnight at 4°C. The stomach muscularis was prepared as whole mounts for immediate immunostaining. Cryoprotected brains were sectioned at 25 µm using a freezing microtome (1:5 series). The brain sections were collected in 0.1 M PBS (pH 7.4), then transferred in a cryoprotectant solution (30% sucrose, 30% ethylene glycol), and stored at −20°C. Other cryoprotected tissues were frozen in TissueTek OCT compound (Sakura) on dry ice before being

sectioned at 16 µm using a cryostat (1:5 series). The sections were collected on SuperFrost slides and stored at −80°C.

Antibody characterization

Table 1 compiles the primary and secondary antibodies used in this study. A discussion relative of the specificity of our primary antibodies is listed below. All of them were commercially available.

Polyclonal rabbit antibody against CART (55-102) (RRID:AB_2313614). We used the residue nomenclature established for rat CART peptides (Rogge et al., 2008). This antiserum was extensively characterized in the CNS and peripheral ganglia, including the nodose ganglion (Zheng et al., 2002; Valera et al., 2006; Gonsalvez et al., 2010; Reeber and Sillitoe, 2011). Controls for specificity included pre-adsorption with a CART (55–102) peptide and omission of the primary antibody (Dun et al., 2000; Reeber and Sillitoe, 2011). According to the manufacturer, this antibody detects a 5 Kda band on western blot of rat brain samples. CART staining in both the brain and nodose ganglion samples displayed a distribution pattern that perfectly agreed with previous reports using this antiserum. The neurons in the nodose ganglion were not stained when the primary antibody was omitted.

We also tested an antibody against CART (1-39) (Phoenix Pharmaceutical Cat#H-003-63; R&D Cat#AF163). However, this antibody failed to label the nodose ganglion and thus we have not included these data in the manuscript. This is not completely surprising since #H-003-063 was raised against a CART fragment that is not very well studied and not considered as biologically relevant as CART (55–102).

Chicken anti-GFP polyclonal antiserum. Many laboratories have used this antibody to label the mouse brain and ganglia of transgenic mice that express GFP and verified the absence of staining when it was used against wildtype tissue (Volkmann et al., 2010; Marques-Lopes et al., 2014). In addition, GFP-expressing hippocampal neurons showed endogenous fluorescence that was only enhanced by immunostaining with the antiserum (Yi et al., 2015).

Peripherin polyclonal antiserum. According to the manufacturer, this antiserum is regularly tested on PC12 lysates and detects a major band at 57 kDa. Lysates from cell lines transfected with the peripherin gene also showed a single band of approximately 58 kDa (Tseng et al., 2008; Xiao et al., 2008). Moreover, it was shown that the staining obtained with this antibody overlapped perfectly with that of eGFP-peripherin in PC12 cells (Tseng et al., 2008). As anticipated, this antibody produced filamentous staining of the neuronal perikarya in the nodose ganglion. Here, we used peripherin as a pan-neuronal marker for vagal afferents.

Polyclonal goat antiserum against TH (RRID:AB_10710873). The data from the manufacturer show that this antiserum detects a single 50 kDa band from rat, mouse and human brain lysates. This antibody has been used to label the mouse striatum and the rat ventral tegmental area (Garcia-Perez et al., 2013; Biezonski et al., 2015). Omission of the antibody resulted in no staining. Here, we used the TH antibody to label subsets of postsynaptic neurons in the dorsovagal complex. In our samples, this antiserum produced a staining pattern that was consistent with the distribution of TH-positive neurons in the mouse dorsovagal complex (Cork et al., 2015).

Polyclonal goat anti pro-MCH (RRID:AB_2237276). By western blot (see manufacturer's sheet), this antibody detects one band of 45-50 KDa. Although the exact sequence of the immunogenic peptide is not available, Deurveilher and colleagues (Deurveilher et al., 2006) have discussed the observation that this antibody certainly detected MCH neurons in the lateral hypothalamus. For instance, they showed overlapping staining with another antibody (same as below) and a lack staining when the antibody was preadsorbed with the immunogen peptide (Deurveilher et al., 2006). Moreover, this antiserum did not label orexin-positive cells. In our laboratory, this antiserum exclusively labeled neurons in the lateral hypothalamus region, strongly suggesting specificity. The lateral hypothalamus was not stained when the primary antibody was omitted. Finally, another group showed that this antiserum did not immunolabel structures in mice lacking MCH neurons (Whiddon and Palmiter, 2013), further exhibiting its specificity.

Polyclonal rabbit antiserum against MCH (RRID:AB_10013632). According to Deurveihler and colleagues (Deurveilher et al., 2006), this antibody labels exactly the same cells as the pro-MCH antibody described above. The manufacturer also performed competitive radioimmunoassays to ascertain specificity. Incubation of the primary antibody with its immunogenic peptide prevented the labeling of the rat brain (Glavas et al., 2008). In this study, the distribution pattern of the MCH-positive elements observed in the mouse brain was consistent with that described by other groups using other antibodies against MCH (Croizier et al., 2010).

Double fluorescent immunohistochemistry

The native fluorescence for ChR2-YFP was directly observed in the nodose ganglion and brainstem. In peripheral tissues, YFP was indirectly detected using an antiserum against GFP. After rinsing in phosphate-buffered saline (PBS), free-floating brain sections, whole mounts or histological slides were incubated with primary antibodies (diluted in 3% normal donkey serum (NDS; Jackson ImmunoResearch, West Grove, PA cat No, 0.3% Triton X-100 in PBS) at room temperature for 16 to 24 hours. After several PBS washes, the tissues were then incubated with 1:500-1:1,000 dilutions of the appropriate secondary antibodies for 1 hour. The tissue was then covered with Vectashield hard set mounting medium with DAPI (H1500) and coverslipped. **Table 1** summarizes the combinations of primary and secondary antibodies used in this study. Immunohistochemistry was performed at room temperature with gentle horizontal shaking.

In situ hybridization (ISH)

The tissue was processed for chromogenic ISH using the RNAscope 2.5 HD Assay (Brown) from Advanced Cell Diagnostic (Newark, CA). The hypothalami and left nodose ganglia from fed and fasted C57Bl/6 mice were rapidly removed and directly frozen on a bed of dry ice. Fresh-frozen tissue was sectioned at 14 µm using a cryostat and collected on SuperFrost slides. Following the manufacturer's protocol, the tissue was fixed in 10% formalin and was pretreated with a protease-based solution (pretreatment 4) followed by hybridization at 40°C for 2 h in a humidity oven with the double-Z oligo probes for prepro-CART and prepro-MCH listed in **Table 2**. Signal amplification was achieved using DAB and the tissue was counterstained with hematoxylin. Finally, hybridized slides were dehydrated in graded alcohols, immerged in xylene, and coverslipped with Permaslip mounting medium (Alban Scientific, St. Louis, MO).

Confocal imaging and photomicrograph production

Samples from $Na_v1.8$-Cre-ChR2-YFP mice were scanned using a Leica SP5 confocal microscope. Oil immersion 40x and 63x objectives were used. The gain and laser intensity were slightly adjusted for each tissue. However, the same scanning parameters were applied when comparing the same tissues from different feeding groups. The line average was 8 or 16. The step increase in the z-axis was usually 0.35 µm, and the total number of optical sections in each stack was 10-20. Most of the images in the manuscript were merged into one color and projected onto a single plane, unless mentioned otherwise in the legend. Single optical sections were used for the estimates and colocalization studies. ImageJ (http://rsb.info.nih.gov/ij/) was used to convert all our confocal-acquired images (lif format) into TIFF images (RGB, 300 dpi) and generate scale bars. CART-positive cells were subjectively evaluated by scaling cell profiles clearly containing immunoreactivity within the outline of the YFP-labeled structures that conformed well to the shapes of these structures.

Adobe Photoshop CS5.1 (Adobe Systems, San Jose, CA) was used to combine the digital images into annotated plates. In some instances, several images were stitched together, as indicated in the legend. The contrast and brightness were uniformly adjusted by adding one adjustment layer. Finally, DAPI-labeled structures were converted to grey scale for better contrast and red–green fluorescence images were converted to magenta–green for color-blind readers.

Estimates of double labeled cells and axons. We estimated the percentage of ChR2-YFP-labeled vagal afferents by counting the cell profiles that were double-labeled for peripherin and ChR2-YFP. Likewise, we counted the neurons that were double labeled for CART and ChR2-YFP in the nodose ganglion. A neuron was considered double labeled when the shape of the YFP-positive profile corresponded to that of the CART or peripherin-stained profiles. The neurons were counted in digital images obtained with a Zeiss microscope (Imager ZI, 20× objective) equipped with a scanning stage and attached to the ApoTome system and a digital camera (Axiocam MRm). A desktop computer running Axiovision 4.7 was used to produce the digital images. The neurons in a 1:5 series of sections across the nodose ganglion were counted by a blinded observer. To evaluate the relative intensity of fluorescence in CART-labeled cells, we used a method described in the literature with slight modifications (Fang et al., 2002). Using ImageJ, the mean absorbance of outlined CART-positive profiles was measured using measurement tools. The average of the mean absorbance of one negative profile in each tissue section of chow-fed mice was used as our 0% intensity (a). The average of the mean absorbance of one most intensely stained profile in each tissue section of chow-fed mice was used as 100% intensity (b). The intensity of the measured profiles was scaled between the minimal and maximal values as follows:

Relative intensity of CART-labeled profile = (measured mean - a)/(b - a)*100.

The measurements were repeated in a large number of individual cell profiles as indicated in our graph. Data were expressed as the relative intensity (%) of individual CART cells compared to the darkest stained cells. This method allowed us to easily visualize the full range of immunoreactivity of CART cells across our different feeding groups. Cell profiles were categorized according to their relative immunoreactivity as containing low (between 0 and 25%), medium (between 25 and 75%), or high immunoreactivity (75% and over 100%). Finally, we calculated the frequency of neurons falling into each category across feeding groups. None of the estimates described above were meant to provide absolute counts, but relative estimates across different feeding conditions. Thus, we did not correct our data for

double counting, and did not use the stereological technique use. The graphs were constructed using GraphPad Prism 7.01.

The estimates described below were performed in a 1:5 series of sections using digital images of single optical sections acquired with a confocal microscopy (63x, zoom 6). Counting was performed by a blinded experimenter. The percentage of CART-positive varicosities in the AP was evaluated. Double-labeled varicosities were considered when CART staining was clearly contained within the boundaries of each ChR2-YFP-labeled varicosity. Second, the diameters of the ChR2-YFP-labeled axons and varicosities in the AP were evaluated. The counts and measurements were collected using ImageJ measuring tools.

Immunofluorescence in the rat was captured using a digital camera (Axiocam) attached to a Zeiss microscope Imager ZI equipped with the Apotome system. Several images of the rat nodose ganglion taken at 40x were stitched together using the Axiovision 4.7 software. The density of CART-positive cells in the rat nodose ganglion was evaluated using Axiovision 4.7. A blinder observer manually counted the number of cell profiles that were immunoreactive for CART. The number of profiles was divided by the surface of tissue occupied by the nodose ganglion.

ISH signals for prepro-CART mRNA were analyzed on DAB-labeled ganglia counterstained with hematoxylin. Images were taken using the brightfield optics of the Zeiss Axioskop 2 microscope and the Axiovision 4.8 software. The percentage of prepro-CART-expressing profiles was estimated by manually counting clearly identifiable neuronal profiles with or without DAB. The intensity of the hybridization signals was further evaluated by subjectively scaling neuronal profiles with low (less than 20 DAB-positive dots per profile), medium (dense accumulation of DAB with large areas of the cytoplasm still visible), or high signals (dense accumulation of DAB covering almost entirely the cell profile). We then calculated the frequency of profiles falling into each category across feeding groups.

Results

Tracing the vagal afferents using the $Na_v1.8$-Cre-ChR2-YFP mice.

We first tried to establish the usefulness of $Na_v1.8$-Cre-ChR2-YFP mice in labeling the vagal C-fibers. In the nodose ganglion, the soma of the vagal afferents and their proximal axons showed robust endogenous green fluorescence (**Figure 1A**). ChR2-YFP was clearly visible, without the need for immunostaining, in the membrane and cytoplasm of many vagal afferents (**Figure 1A, B**). We estimated that 82% ± 2 (n=4) of the vagal afferents that stained for peripherin, a pan-neuronal marker in the peripheral nervous system (Gorham et al., 1990), were also positive for ChR2-YFP (**Figure 1B-D**).

In addition, ChR2-YFP labeled the membranes of the vagal terminals within the dorsovagal complex (**Figure 2A; Figure 3**). Although we observed a few isolated ChR2-YFP-labeled neurons in the forebrain (mainly in the cortex and striatum), no neurons were detected in the hypothalamus or brainstem (not shown). Thus, the ChR2-YFP-labeled fibers observed in the dorsovagal complex were essentially derived from the nodose ganglion. The densest innervation was observed in the dorsal and medial parts of the NTS, as well as the solitary tract itself (**Figure 2A**). Innervation was less dense in the AP and other parts of the NTS (**Figure 2A**). The innervation of the dorsovagal complex was very dense, forming bundles of intermingled axons circling the putative location of the postsynaptic neurons. For example,

ChR2-YFP varicosities accumulated in the vicinity of tyrosine hydroxylase (TH)-positive neurons in the AP and NTS (**Figure 2B**). Although it was difficult to distinguish individual axons and varicosities at low magnification, optical sectioning at higher magnification (63x) revealed individual thin axons (average diameter of 0.3 ± 0.0 µm; n=3) decorated with boutons and varicosities resembling presynaptic terminals (average diameter of 0.9 ± 0.0 µm; n=3) (**Figure 2C**). **Movie 1** is a file compilation of a Z-stack of ChR2-YFP-labeled axons (green) around one TH-positive neuron (red).

ChR2-YFP was also transported toward peripheral tissues that were innervated by C-fibers (**Figure 4**). However, the native fluorescence for ChR2-YFP was much weaker in the periphery than in the ganglia or brain. For instance, low to nearly undetectable levels of endogenous YFP fluorescence were seen in the epidermis (**Figure 4A**) and intestinal mucosa (**Figure 4C**). Immunostaining with an anti-GFP antiserum successfully marked axons and specialized sensory endings in the aforementioned tissues (**Figure 4B, D**). Thus, the subsequent experiments depicting ChR2-YFP in the peripheral tissues were performed using GFP immunofluorescence. Overall, $Na_v1.8$-Cre-ChR2-YFP mice allowed the assessment of the detailed morphology of C-fibers in many visceral tissues (not shown). Importantly, no cell bodies were ever labeled in peripheral organs.

Distribution and regulation of CART in vagal afferents of metabolically challenged mice.

In the nodose ganglion of the $Na_v1.8$-Cre-ChR2-YFP mice, immunoreactivity for CART (55-102) was detected in the soma and proximal axons of many neurons (**Figure 5A, C; Figure 6**). The nodose ganglion neurons were not stained when the CART primary antibody was omitted (**Figure 5B**). In agreement with previous works (Broberger et al., 1999; Zheng et al., 2002; Scruggs et al., 2003), immunoreactivity for CART was evident in large puncta around the cell nucleus and within the proximal axon (**Figure 5B**). Approximately 55% of ChR2-YFP-labeled neurons were CART-positive (**Figure 6; Figure 7A**) and over 99% of the CART-positive cells were labeled with ChR2-YFP. The CART staining in the nodose ganglion looked identical in fed, fasted and obese animals when observed under blinded conditions (**Figure 6A-F**). According to our estimates, the percentage of ChR2-YFP-labeled neurons containing CART was identical across the feeding groups (**Figure 7A**). Because CART immunoreactivity varied in intensity between neurons, we also examined the relative intensity of CART (55-102) immunoreactivity in a large number of cell profiles (**Figure 7C**). The percentages of cells with low, medium, and high immunoreactivity were identical across the feeding groups (**Figure 7C**).

Most of the studies on the impact of fasting on vagal CART were performed in rats. To rule out the possibility of species differences, were examined CART in fed and fasted rats (**Figure 8**). The distribution and intensity of the CART staining in the nodose ganglion looked identical in fed and fasted rats when observed under blinded conditions (**Figure 8**). Moreover, the density of CART-positive profiles across the ganglion was not significantly different in fed (125 ± 18 cells/mm^2, n=3) and fasted rats (160 ± 27 cells/mm^2, n=3).

We also assessed CART immunoreactivity in the vagal terminals in the dorsovagal complex. CART (55-102) immunoreactivity was observed throughout the entire dorsovagal complex and included both neuronal soma and fibers (**Figure 9A**). Across the feeding groups, the distribution and intensity of CART immunoreactivity was directly comparable (**Figure 9A-C**). CART immunoreactivity was observed in ChR2-YFP axons and varicosities in the area postrema (AP) and commissural part of the nucleus of the solitary tract (SolC), in agreement with the results of Zheng and colleagues (Zheng et al., 2002). In these

regions, CART immunoreactivity corresponded well to the shape of the YFP-labeled varicosities (**Figure 9G, H**). However, not all CART-positive elements corresponded to YFP-labeled structures, and in other parts of the dorsovagal complex, double-labeled axons were rarely observed (not shown). In the AP, CART (55-102) was present in approximately 22% of the ChR2-YFP-labeled varicosities (**Figure 7B**). In agreement with our results in the nodose ganglion, our estimates showed identical percentages of varicosities that were co-labeled for CART and ChR2-YFP in the AP of the fed, fasted, and high-fat diet fed animals (**Figure 7B**). As a remark, we did not notice obvious differences in the shape, amount, and distribution of ChR2-YFP-labeled fibers across the feeding groups (**Figure 9D-F**).

Lastly, we also assessed the expression of prepro-CART mRNA in the nodose ganglia of fed and fasted wild-type mice. Using chromogenic ISH, prepro-CART mRNA was detected at high levels in select hypothalamic nuclei known to express CART (**Figure 10A**). Robust signals for prepro-CART mRNA were also present in nodose ganglia of the fed and fasted mice (**Figure 10B, C**). Variable amount of DAB accumulated in the soma of many vagal sensory neurons, including in the fasted condition (**Figure 10D**). The percentage of prepro-CART-expressing cells and the relative intensity of hybridization signal per cell did not significantly change after fasting (**Figure 7D**).

Absence of MCH in vagal afferents of metabolically challenged mice.

Because MCH has been reported to be produced in CART afferents in response to fasting, we sought to evaluate the presence of both pro-MCH and MCH in our mice. First, we used an antiserum against pro-MCH that preferentially stained the perikarya. We successfully detected immunoreactivity for prepro-MCH in the perikarya of neurons in the lateral hypothalamus (**Figure 11A**). The lateral hypothalamus neurons were not stained when the pro-MCH antibody was omitted (not shown). We were unable to see any immunoreactivity for pro-MCH in the nodose ganglion of $Na_v1.8$-Cre-ChR2-YFP mice, even in the fasted mice (**Figure 11B**). Identical results were obtained in samples incubated with higher concentrations of antibody (up to 1/100) (data not shown). Second, we used an antiserum against MCH itself. MCH immunoreactivity was observed in axons across the forebrain. However, the dorsovagal complex of the fed, fasted and obese animals contained very little MCH (**Figure 11C, D**). Typically, isolated MCH-positive varicose axons were observed in the ventral region of the medial part of the nucleus of the solitary tract (SolM), where the YFP-labeled fibers were relatively sparse (**Figure 11C, D**). These MCH-positive axons never colocalized with YFP-labeled axons, further confirming that vagal afferents do not produce MCH. To rule out the possibility of species differences, we also examined pro-MCH in the nodose ganglion of fed and fasted rats. Consistent with our mouse data, we were not able to detect immunoreactivity (data not shown).

To rule out the possibility of a false-negative result, we also assessed the expression of prepro-MCH mRNA in the nodose ganglia of fed and fasted wild-type mice. As expected, chromogenic ISH revealed very intense signals in the lateral hypothalamus (**Figure 10E**). In contrast, the rest of the brain and the nodose ganglion were completely devoid of signal, regardless of the nutritional status of the mice (**Figure 10F-H**).

Absence of CART immunoreactivity in gastrointestinal endings

In the vagus nerve itself, we did not observe CART immunoreactivity any YFP-labeled axons (**Figure 12A**). In the gastrointestinal tract, abundant CART immunoreactivity was observed, likely originating from post-ganglionic neurons (Calupca et al., 2001; Ekblad et al., 2003; Gonsalvez et al., 2010) and vagal efferents (Zheng et al., 2002). In those tissues, CART staining was observed in enteric neurons and fibers running closely to ChR2-YFP axons. However, CART did not colocalize with YFP-labeled axons themselves. For instance, ChR2-YFP-labeled specialized endings resembling vagal intraganglionic laminar endings were CART negative (**Figure 12B**). Similar observations were reported in the duodenal mucosa (not shown). This suggested that CART is not efficiently transported to the peripheral sensory endings of C-fibers including those in the vagus nerve.

Discussion

The present study characterized CART (55-102) immunoreactivity in the vagal afferents of $Na_v1.8$-Cre-ChR2-YFP mice. Our results indicated that CART (55-102) is constitutively expressed in approximately 55% of the vagal $Na_v1.8$-expressing neurons, even in the fasted mice. MCH, a peptide that was previously reported to be induced in CART-positive vagal afferents of fasted animals, was undetectable. In contrast to several studies, we concluded that the neuropeptidergic profile of the CART-positive vagal afferents is remarkably stable across the energy balance spectrum.

Technical considerations. We used reporter mice that invariably express ChR2-YFP in $Na_v1.8$-Cre-expressing cells to label C-fibers in their entirety. $Na_v1.8$-Cre mice crossed with either tdTomato or ChR2 reporter animals have previously been utilized to label the perikarya and axons of C-fibers, including somatosensory nociceptors (Gautron et al., 2011; Shields et al., 2012; Daou et al., 2013; Bonin et al., 2016). To our knowledge, this is the first study to use $Na_v1.8$-Cre-ChR2-YFP mice to describe visceral C-fibers. Overall, our data further validate the usefulness of ChR2-YFP as an excellent neuronal tracer. In particular, ChR2-YFP presented the advantage of brightly labeling the membrane of both central and peripheral endings, thereby allowing the tracing of specialized endings at high resolution. In the dorsovagal complex, this approach was critical for distinguishing the axons of vagal origins from central axons. A minor caveat of this mouse model is that GFP immunohistochemistry was required to detect ChR2-YFP in peripheral tissues, probably due to its limited peripheral transport. In the past, isolectin B4 binding to C-fiber neurons has been commonly employed to trace the perikarya and central axons of C-fiber neurons (Fang et al., 2006; Fullmer et al., 2007; Solorzano et al., 2015). However, due to extraneuronal binding (Kirkeby and Moe, 2001), isolectin B4 does not permit the labeling of axons that innervate peripheral tissues. In addition, numerous developmental, biological and inflammatory factors influence Isolectin B4 binding to sensory neurons (Beland and Fitzgerald, 2001; Fullmer et al., 2007); Therefore, it is possible that isolectin B4 binding to C-fibers may vary in response to different physiological conditions.

In contrast to several previous studies (de Lartigue et al., 2007; De Lartigue et al., 2010; de Lartigue et al., 2014), we did not observe any suppression of CART immunoreactivity in response to fasting, even though we used the same antibodies. However, our mouse data are in agreement with our ISH and the results of Broberger and colleagues, who investigated the regulation of the CART mRNA in metabolically challenged rats (Broberger et al., 1999). Importantly, the number and appearance of CART-labeled cells were consistent with the published literature (Broberger et al., 1999; Zheng et al., 2002; Scruggs et al., 2003). In addition, abundant CART immunoreactivity was also observed in the nodose

ganglion of fasted rat. Together, these observations made us confident that the CART immunostaining observed in our study, including in the fasted mice, was not the result of false-positive labeling. Likewise, our failure to detect MCH in the nodose ganglion was not likely due to false-negative results because we employed well-characterized antisera that successfully stained the brain. If MCH had been truly produced in the nodose ganglion of fasted animals, then we should have been able to detect it in the vagal terminals of the dorsovagal complex. More importantly, prepro-MCH mRNA was completely undetectable in the mouse nodose ganglion, even in the fasted condition. The absence of MCH in vagal afferents is consistent with the fact that the administration of MCH in the 4th ventricle does not influence food intake (Zheng et al., 2005; Baird et al., 2008). Even though differences in age, strain, bleeds of antibody, and diets may have influenced our results, we are confident that MCH is not produced by the vagal afferents.

Regarding the neuropeptidergic make-up of the vagal afferents. Although many different neuropeptides have been described in vagal afferents, the majority of them are expressed at relatively low levels and/or expressed in small numbers of neurons, which is true for substance P, galanin, neuropeptide Y, and CGRP (Helke and Niederer, 1990; Calingasan and Ritter, 1992; Kummer et al., 1993; Matsumoto et al., 2003; Young et al., 2008). Of note, the aforementioned peptides are often produced by vagal afferents innervating the lungs (Undem et al., 2004; Plato et al., 2006) and therefore are not necessarily involved in feeding regulation. This contrasts sharply with CART, which is abundantly expressed in many vagal afferents, including those involved in feeding. Furthermore, our results indicate that CART expression in the nodose ganglion is not influenced by metabolic challenges. This result is not entirely surprising because few physiological or pathophysiological stimuli have been reported to modify neuropeptide expression in vagal afferents, with the notable exception of the peripheral axotomy (Zhang et al., 1996; Reimer and Kanje, 1999). Hence, the neuropeptidergic profiles of the CART-positive hypothalamic neurons and CART-positive vagal afferents are substantially different. For instance, hypothalamic CART neurons often co-express several feeding-related peptides (Elias et al., 1998). Moreover, hypothalamic CART expression is significantly altered by metabolic challenges, including food restriction (Kristensen et al., 1998) and high-fat diet feeding (Lee et al., 2013). Nonetheless, even in the hypothalamus, we are not aware of neurons switching from being anorectic to being orexigenic.

Most published studies agree that approximately 40-50% of the neurons are immunoreactive for CART in rats and mice in the fed condition (Zheng et al., 2002; de Lartigue et al., 2007; Gautron et al., 2012). Using radioactive ISH, approximately 48% of the vagal afferents were found to express CART in the rat (Broberger et al., 1999). However, using chromogenic ISH, we found that approximately 67% of the mouse vagal afferents expressed CART. This is likely due to the fact that the RNAscope technology is not only more sensitive than immunofluorescence but also provides better signal-to-noise ratio than radioactive ISH (Wang et al., 2012). Nonetheless, species differences in the distribution and percentage of vagal afferents expressing neuropeptides have been reported in the nodose ganglion of rats and mice (Zhuo et al., 1997). Therefore, we cannot completely rule out that CART mRNA is expressed in more vagal afferents in the mouse than in the rat. However, our current data in both species combined with that of Broberger and colleagues (Broberger et al., 1999) support the view that vagal CART is not regulated by fasting.

462 **Localization of CART in vagal terminals.** Many neuropeptides, including vasoactive intestinal
463 peptide and calcitonin gene-related peptide, are known to be transported from the cell body of vagal
464 afferents to their peripheral terminals (Zhuo et al., 1995). We expected to find CART in C-fiber terminals
465 located in the stomach and duodenum because previous studies clearly showed that CART-positive vagal
466 afferents project to these locations (Zheng et al., 2002). Surprisingly, we failed to detect CART
467 immunoreactivity in the axons and peripheral endings of vagal neurons that innervate the stomach wall
468 and duodenal mucosa. We concluded that CART was not efficiently transported to the vagal endings and,
469 consequently, may serve mainly as a central neurotransmitter. However, we cannot entirely rule out that
470 our study missed CART immunoreactivity in the gastrointestinal tract. Further tracing studies are
471 therefore warranted to determine the projection sites of CART-positive vagal afferents in both thoracic
472 and abdominal viscera.

473

474

475

476 Aja S, Robinson BM, Mills KJ, Ladenheim EE, Moran TH (2002) Fourth ventricular CART reduces food and
477 water intake and produces a conditioned taste aversion in rats. Behavioral neuroscience
478 116:918-921.
479 Baird JP, Rios C, Loveland JL, Beck J, Tran A, Mahoney CE (2008) Effects of hindbrain melanin-
480 concentrating hormone and neuropeptide Y administration on licking for water, saccharin, and
481 sucrose solutions. Am J Physiol Regul Integr Comp Physiol 294:R329-343.
482 Beland B, Fitzgerald M (2001) Influence of peripheral inflammation on the postnatal maturation of
483 primary sensory neuron phenotype in rats. The journal of pain : official journal of the American
484 Pain Society 2:36-45.
485 Biezonski DK, Trifilieff P, Meszaros J, Javitch JA, Kellendonk C (2015) Evidence for limited D1 and D2
486 receptor coexpression and colocalization within the dorsal striatum of the neonatal mouse. J
487 Comp Neurol 523:1175-1189.
488 Bonin RP, Wang F, Desrochers-Couture M, Ga Secka A, Boulanger ME, Cote DC, De Koninck Y (2016)
489 Epidural optogenetics for controlled analgesia. Molecular pain 12.
490 Broberger C, Holmberg K, Kuhar MJ, Hokfelt T (1999) Cocaine- and amphetamine-regulated transcript in
491 the rat vagus nerve: A putative mediator of cholecystokinin-induced satiety. Proc Natl Acad Sci U
492 S A 96:13506-13511.
493 Burdyga G, Varro A, Dimaline R, Thompson DG, Dockray GJ (2006) Feeding-dependent depression of
494 melanin-concentrating hormone and melanin-concentrating hormone receptor-1 expression in
495 vagal afferent neurones. Neuroscience 137:1405-1415.
496 Calingasan NY, Ritter S (1992) Presence of galanin in rat vagal sensory neurons: evidence from
497 immunohistochemistry and in situ hybridization. J Auton Nerv Syst 40:229-238.
498 Calupca MA, Locknar SA, Zhang L, Harrison TA, Hoover DB, Parsons RL (2001) Distribution of cocaine-
499 and amphetamine-regulated transcript peptide in the guinea pig intrinsic cardiac nervous
500 system and colocalization with neuropeptides or transmitter synthetic enzymes. J Comp Neurol
501 439:73-86.
502 Chiu IM, Barrett LB, Williams EK, Strochlic DE, Lee S, Weyer AD, Lou S, Bryman GS, Roberson DP,
503 Ghasemlou N, Piccoli C, Ahat E, Wang V, Cobos EJ, Stucky CL, Ma Q, Liberles SD, Woolf CJ (2014)
504 Transcriptional profiling at whole population and single cell levels reveals somatosensory
505 neuron molecular diversity. eLife 3.
506 Cork SC, Richards JE, Holt MK, Gribble FM, Reimann F, Trapp S (2015) Distribution and characterisation
507 of Glucagon-like peptide-1 receptor expressing cells in the mouse brain. Molecular metabolism
508 4:718-731.
509 Croizier S, Franchi-Bernard G, Colard C, Poncet F, La Roche A, Risold PY (2010) A comparative analysis
510 shows morphofunctional differences between the rat and mouse melanin-concentrating
511 hormone systems. PloS one 5:e15471.
512 Daou I, Tuttle AH, Longo G, Wieskopf JS, Bonin RP, Ase AR, Wood JN, De Koninck Y, Ribeiro-da-Silva A,
513 Mogil JS, Seguela P (2013) Remote optogenetic activation and sensitization of pain pathways in
514 freely moving mice. J Neurosci 33:18631-18640.
515 de La Serre CB, de Lartigue G, Raybould HE (2015) Chronic exposure to low dose bacterial
516 lipopolysaccharide inhibits leptin signaling in vagal afferent neurons. Physiol Behav 139:188-194.
517 de Lartigue G, Ronveaux CC, Raybould HE (2014) Deletion of leptin signaling in vagal afferent neurons
518 results in hyperphagia and obesity. Molecular metabolism 3:595-607.
519 de Lartigue G, Dimaline R, Varro A, Dockray GJ (2007) Cocaine- and amphetamine-regulated transcript:
520 stimulation of expression in rat vagal afferent neurons by cholecystokinin and suppression by
521 ghrelin. J Neurosci 27:2876-2882.

522 De Lartigue G, Dimaline R, Varro A, Raybould H, De la Serre CB, Dockray GJ (2010) Cocaine- and
523 amphetamine-regulated transcript mediates the actions of cholecystokinin on rat vagal afferent
524 neurons. Gastroenterology 138:1479-1490.
525 Deurveilher S, Lo H, Murphy JA, Burns J, Semba K (2006) Differential c-Fos immunoreactivity in arousal-
526 promoting cell groups following systemic administration of caffeine in rats. J Comp Neurol
527 498:667-689.
528 Dun NJ, Dun SL, Wong PY, Yang J, Chang J (2000) Cocaine- and amphetamine-regulated transcript
529 peptide in the rat epididymis: an immunohistochemical and electrophysiological study. Biology
530 of reproduction 63:1518-1524.
531 Ekblad E, Kuhar M, Wierup N, Sundler F (2003) Cocaine- and amphetamine-regulated transcript:
532 distribution and function in rat gastrointestinal tract. Neurogastroenterol Motil 15:545-557.
533 Elias CF, Lee C, Kelly J, Aschkenasi C, Ahima RS, Couceyro PR, Kuhar MJ, Saper CB, Elmquist JK (1998)
534 Leptin activates hypothalamic CART neurons projecting to the spinal cord. Neuron 21:1375-
535 1385.
536 Fang X, Djouhri L, Black JA, Dib-Hajj SD, Waxman SG, Lawson SN (2002) The presence and role of the
537 tetrodotoxin-resistant sodium channel Na(v)1.9 (NaN) in nociceptive primary afferent neurons. J
538 Neurosci 22:7425-7433.
539 Fang X, Djouhri L, McMullan S, Berry C, Waxman SG, Okuse K, Lawson SN (2006) Intense isolectin-B4
540 binding in rat dorsal root ganglion neurons distinguishes C-fiber nociceptors with broad action
541 potentials and high Nav1.9 expression. J Neurosci 26:7281-7292.
542 Fullmer JM, Riedl M, Williams FG, Sandrin M, Elde R (2007) Enzymes that synthesize the IB4 epitope are
543 not sufficient to impart IB4 binding in dorsal root ganglia of rat. J Comp Neurol 501:70-82.
544 Garcia-Perez D, Saez-Belmonte F, Laorden ML, Nunez C, Milanes MV (2013) Morphine administration
545 modulates expression of Argonaute 2 and dopamine-related transcription factors involved in
546 midbrain dopaminergic neurons function. British journal of pharmacology 168:1889-1901.
547 Gautron L, Lee CE, Lee S, Elmquist JK (2012) Melanocortin-4 receptor expression in different classes of
548 spinal and vagal primary afferent neurons in the mouse. J Comp Neurol 520:3933-3948.
549 Gautron L, Sakata I, Udit S, Zigman JM, Wood JN, Elmquist JK (2011) Genetic tracing of Nav1.8-
550 expressing vagal afferents in the mouse. J Comp Neurol 519:3085-3101.
551 Glavas MM, Grayson BE, Allen SE, Copp DR, Smith MS, Cowley MA, Grove KL (2008) Characterization of
552 brainstem peptide YY (PYY) neurons. J Comp Neurol 506:194-210.
553 Gonsalvez DG, Kerman IA, McAllen RM, Anderson CR (2010) Chemical coding for cardiovascular
554 sympathetic preganglionic neurons in rats. J Neurosci 30:11781-11791.
555 Gorham JD, Baker H, Kegler D, Ziff EB (1990) The expression of the neuronal intermediate filament
556 protein peripherin in the rat embryo. Brain Res Dev Brain Res 57:235-248.
557 Heldsinger A, Lu Y, Zhou SY, Wu X, Grabauskas G, Song I, Owyang C (2012) Cocaine- and amphetamine-
558 regulated transcript is the neurotransmitter regulating the action of cholecystokinin and leptin
559 on short-term satiety in rats. Am J Physiol Gastrointest Liver Physiol 303:G1042-1051.
560 Helke CJ, Niederer AJ (1990) Studies on the coexistence of substance P with other putative transmitters
561 in the nodose and petrosal ganglia. Synapse 5:144-151.
562 Jennings JH, Stuber GD (2014) Tools for resolving functional activity and connectivity within intact neural
563 circuits. Current biology : CB 24:R41-50.
564 Kirkeby S, Moe D (2001) Binding of Griffonia simplicifolia 1 isolectin B4 (GS1 B4) to alpha-galactose
565 antigens. Immunology and cell biology 79:121-127.
566 Koylu EO, Couceyro PR, Lambert PD, Ling NC, DeSouza EB, Kuhar MJ (1997) Immunohistochemical
567 localization of novel CART peptides in rat hypothalamus, pituitary and adrenal gland. J
568 Neuroendocrinol 9:823-833.

569 Kristensen P, Judge ME, Thim L, Ribel U, Christjansen KN, Wulff BS, Clausen JT, Jensen PB, Madsen OD,
570 Vrang N, Larsen PJ, Hastrup S (1998) Hypothalamic CART is a new anorectic peptide regulated by
571 leptin. Nature 393:72-76.
572 Kummer W, Bachmann S, Neuhuber WL, Hanze J, Lang RE (1993) Tyrosine-hydroxylase-containing vagal
573 afferent neurons in the rat nodose ganglion are independent from neuropeptide-Y-containing
574 populations and project to esophagus and stomach. Cell Tissue Res 271:135-144.
575 Lee SJ, Verma S, Simonds SE, Kirigiti MA, Kievit P, Lindsley SR, Loche A, Smith MS, Cowley MA, Grove KL
576 (2013) Leptin stimulates neuropeptide Y and cocaine amphetamine-regulated transcript
577 coexpressing neuronal activity in the dorsomedial hypothalamus in diet-induced obese mice. J
578 Neurosci 33:15306-15317.
579 Madisen L, Zwingman TA, Sunkin SM, Oh SW, Zariwala HA, Gu H, Ng LL, Palmiter RD, Hawrylycz MJ,
580 Jones AR, Lein ES, Zeng H (2010) A robust and high-throughput Cre reporting and
581 characterization system for the whole mouse brain. Nat Neurosci 13:133-140.
582 Marques-Lopes J, Van Kempen T, Waters EM, Pickel VM, Iadecola C, Milner TA (2014) Slow-pressor
583 angiotensin II hypertension and concomitant dendritic NMDA receptor trafficking in estrogen
584 receptor beta-containing neurons of the mouse hypothalamic paraventricular nucleus are sex
585 and age dependent. J Comp Neurol 522:3075-3090.
586 Matsumoto I, Emori Y, Nakamura S, Shimizu K, Arai S, Abe K (2003) DNA microarray cluster analysis
587 reveals tissue similarity and potential neuron-specific genes expressed in cranial sensory ganglia.
588 J Neurosci Res 74:818-828.
589 Munoz W, Tremblay R, Rudy B (2014) Channelrhodopsin-assisted patching: in vivo recording of
590 genetically and morphologically identified neurons throughout the brain. Cell reports 9:2304-
591 2316.
592 Plato M, Kummer W, Haberberger RV (2006) Structural and neurochemical comparison of vagal and
593 spinal afferent neurons projecting to the rat lung. Neurosci Lett 395:215-219.
594 Reeber SL, Sillitoe RV (2011) Patterned expression of a cocaine- and amphetamine-regulated transcript
595 peptide reveals complex circuit topography in the rodent cerebellar cortex. J Comp Neurol
596 519:1781-1796.
597 Reimer M, Kanje M (1999) Peripheral but not central axotomy promotes axonal outgrowth and induces
598 alterations in neuropeptide synthesis in the nodose ganglion of the rat. The European journal of
599 neuroscience 11:3415-3423.
600 Rogge G, Jones D, Hubert GW, Lin Y, Kuhar MJ (2008) CART peptides: regulators of body weight, reward
601 and other functions. Nat Rev Neurosci 9:747-758.
602 Scruggs P, Dun SL, Dun NJ (2003) Cocaine- and amphetamine-regulated transcript peptide attenuates
603 phenylephrine-induced bradycardia in anesthetized rats. Am J Physiol Regul Integr Comp Physiol
604 285:R1496-1503.
605 Shields SD, Ahn HS, Yang Y, Han C, Seal RP, Wood JN, Waxman SG, Dib-Hajj SD (2012) Na(v)1.8
606 expression is not restricted to nociceptors in mouse peripheral nervous system. Pain 153:2017-
607 2030.
608 Solorzano C, Villafuerte D, Meda K, Cevikbas F, Braz J, Sharif-Naeini R, Juarez-Salinas D, Llewellyn-Smith
609 IJ, Guan Z, Basbaum AI (2015) Primary afferent and spinal cord expression of gastrin-releasing
610 peptide: message, protein, and antibody concerns. J Neurosci 35:648-657.
611 Stanley SA, Small CJ, Murphy KG, Rayes E, Abbott CR, Seal LJ, Morgan DG, Sunter D, Dakin CL, Kim MS,
612 Hunter R, Kuhar M, Ghatei MA, Bloom SR (2001) Actions of cocaine- and amphetamine-
613 regulated transcript (CART) peptide on regulation of appetite and hypothalamo-pituitary axes in
614 vitro and in vivo in male rats. Brain Res 893:186-194.
615 Stirling LC, Forlani G, Baker MD, Wood JN, Matthews EA, Dickenson AH, Nassar MA (2005) Nociceptor-
616 specific gene deletion using heterozygous NaV1.8-Cre recombinase mice. Pain 113:27-36.

617 Thim L, Kristensen P, Nielsen PF, Wulff BS, Clausen JT (1999) Tissue-specific processing of cocaine- and
618 amphetamine-regulated transcript peptides in the rat. Proc Natl Acad Sci U S A 96:2722-2727.
619 Tseng KW, Chau YP, Yang MF, Lu KS, Chien CL (2008) Abnormal cellular translocation of alpha-internexin
620 in spinal motor neurons of Dystonia musculorum mice. J Comp Neurol 507:1053-1064.
621 Undem BJ, Chuaychoo B, Lee MG, Weinreich D, Myers AC, Kollarik M (2004) Subtypes of vagal afferent
622 C-fibres in guinea-pig lungs. J Physiol 556:905-917.
623 Usoskin D, Furlan A, Islam S, Abdo H, Lonnerberg P, Lou D, Hjerling-Leffler J, Haeggstrom J, Kharchenko
624 O, Kharchenko PV, Linnarsson S, Ernfors P (2015) Unbiased classification of sensory neuron
625 types by large-scale single-cell RNA sequencing. Nat Neurosci 18:145-153.
626 Valera AG, Cavalcante JC, Elias CF, Felicio LF (2006) Cocaine- and amphetamine-regulated transcript is
627 overexpressed in the anteroventral periventricular nucleus of pregnant rats. J Neuroendocrinol
628 18:711-714.
629 Volkmann K, Chen YY, Harris MP, Wullimann MF, Koster RW (2010) The zebrafish cerebellar upper
630 rhombic lip generates tegmental hindbrain nuclei by long-distance migration in an evolutionary
631 conserved manner. J Comp Neurol 518:2794-2817.
632 Wang F, Flanagan J, Su N, Wang LC, Bui S, Nielson A, Wu X, Vo HT, Ma XJ, Luo Y (2012) RNAscope: a
633 novel in situ RNA analysis platform for formalin-fixed, paraffin-embedded tissues. J Mol Diagn
634 14:22-29.
635 Whiddon BB, Palmiter RD (2013) Ablation of neurons expressing melanin-concentrating hormone (MCH)
636 in adult mice improves glucose tolerance independent of MCH signaling. J Neurosci 33:2009-
637 2016.
638 Xiao S, Tjostheim S, Sanelli T, McLean JR, Horne P, Fan Y, Ravits J, Strong MJ, Robertson J (2008) An
639 aggregate-inducing peripherin isoform generated through intron retention is upregulated in
640 amyotrophic lateral sclerosis and associated with disease pathology. J Neurosci 28:1833-1840.
641 Yi F, Catudio-Garrett E, Gabriel R, Wilhelm M, Erdelyi F, Szabo G, Deisseroth K, Lawrence J (2015)
642 Hippocampal "cholinergic interneurons" visualized with the choline acetyltransferase promoter:
643 anatomical distribution, intrinsic membrane properties, neurochemical characteristics, and
644 capacity for cholinergic modulation. Frontiers in synaptic neuroscience 7:4.
645 Young RL, Cooper NJ, Blackshaw LA (2008) Chemical coding and central projections of gastric vagal
646 afferent neurons. Neurogastroenterol Motil 20:708-718.
647 Zhang X, Ji RR, Arvidsson J, Lundberg JM, Bartfai T, Bedecs K, Hokfelt T (1996) Expression of peptides,
648 nitric oxide synthase and NPY receptor in trigeminal and nodose ganglia after nerve lesions. Exp
649 Brain Res 111:393-404.
650 Zheng H, Patterson LM, Berthoud HR (2002) CART in the dorsal vagal complex: sources of
651 immunoreactivity and effects on Fos expression and food intake. Brain Res 957:298-310.
652 Zheng H, Patterson LM, Morrison C, Banfield BW, Randall JA, Browning KN, Travagli RA, Berthoud HR
653 (2005) Melanin concentrating hormone innervation of caudal brainstem areas involved in
654 gastrointestinal functions and energy balance. Neuroscience 135:611-625.
655 Zhuo H, Ichikawa H, Helke CJ (1997) Neurochemistry of the nodose ganglion. Progress in neurobiology
656 52:79-107.
657 Zhuo H, Lewin AC, Phillips ET, Sinclair CM, Helke CJ (1995) Inhibition of axoplasmic transport in the rat
658 vagus nerve alters the numbers of neuropeptide and tyrosine hydroxylase messenger RNA-
659 containing and immunoreactive visceral afferent neurons of the nodose ganglion. Neuroscience
660 66:175-187.

661

662

Figure 1. Distribution of ChR2-YFP fluorescence in the nodose ganglion of the $Na_v1.8$-Cre-ChR2-YFP mice. **A**: Many neuronal cell bodies and axons were brightly fluorescent in the nodose (NG) and petrosal-jugular ganglion (PJG) (three images were horizontally stitched together). **B–D**: Details of NG peripherin-labeled neurons (AlexaFluor 594). ChR2-YFP is apparent in the membrane and cytoplasm of many NG neurons (but not all) (B). Asterisks are positioned over representative peripherin-positive neurons that were not labeled with ChR2-YFP (B, C). Abbreviations: NG, nodose ganglion; PJG, petrosal-jugular ganglion; X, cervical vagus nerve. Scale bars = 40 μm in A; 20 μm in B (also applies to C,D).

Figure 2. Distribution of ChR2-YFP fluorescence in the dorsovagal complex of the $Na_v1.8$-Cre-ChR2-YFP mice. **A**: Vagal afferents terminating in the area postrema (AP) and nucleus of the solitary tract (NTS) were labeled with ChR2-YFP (3 horizontally stitched images). **B**: Highly varicose ChR2-YFP-labeled axons circling the cell body of one TH-positive neuron (AlexaFluor 594) located in the NTS. **C**: Single optical section of ChR2-YFP-labeled axons in the AP revealing thin varicose axons of varying sizes. Asterisks are positioned over the presumptive locations of the post-synaptic cell bodies, whereas the arrowheads indicate representative vagal varicosities. Abbreviations: AP, area postrema; DMV, dorsal nucleus of the solitary tract; sol, solitary tract; commissural part of the nucleus of the solitary tract; SolDM, dorsomedial part of the nucleus of the solitary tract; SolM, intermediate part of the nucleus of the solitary tract; SubP, subpostrema area. Scale bars = 60 μm in A; 5 μm in B and C.

Movie 1. File compilation of a Z-stack of ChR2-YFP-labeled axons (green) around one TH-positive neuron (AlexaFluor 594) in the area postrema of the $Na_v1.8$-Cre-ChR2-YFP mouse. Note the varicosities in close apposition to the outline of the TH-positive neuron.

Figure 3. Distribution of ChR2-YFP fluorescence throughout the rostrocaudal extension of the dorsovagal complex of one representative $Na_v1.8$-ChR2-YFP mouse. Several digital images were stitched together (epifluorescence with Apotome filter). The number in the bottom right corner indicates the approximate distance from Bregma according to the Franklin and Paxinos Mouse Brain Atlas (3^{rd} edition). Abbreviations: 4v, fourth ventricle; cc, central canal.

Figure 4. Identification of ChR2-YFP-positive fibers in peripheral tissues from the $Na_v1.8$-Cre-ChR2-YFP mice. **A**: Weakly fluorescent structures resembling nerve endings (arrowheads) were observed in the epidermis of the forepaw. **B**: GFP immunolabeling greatly enhanced the labeling of individual axons ramifying into the epidermis. **C**: We could not detect endogenous YFP fluorescence in the duodenal mucosa before immunolabeling. **D**: YFP-labeled axons were evident in the lamina propria (lp) when the tissue was stained for GFP. The antibody produced a small amount of nonspecific background staining in the epithelium (ep). Arrowheads indicate representative YFP-positive fibers. Scale bars = 20 μm in A (also applies to B, C, D).

Figure 5. CART (55-102) detection in the nodose ganglion (NG) of the $Na_v1.8$-Cre-ChR2-YFP mice. **A**: CART-positive cells (AlexaFluor 594) resembling neurons were observed throughout the NG. The two cells located in the inset are represented at high magnification in panel C. **B**: Omission of the primary antibody eliminated CART immunoreactivity. Only a few debris and background could be observed in the NG. **C**: Two adjacent ChR2-YFP-, CART-positive neurons are shown. CART is detected in vesicle-like structures in the cytoplasm and proximal axon. The larger neuron contained more

703 immunoreactivity than the smaller neuron. Two other YFP-labeled neurons did not contain CART. Scale
704 bars = 50 μm in A and B; 5 μm in C.

705 **Figure 6.** CART (55-102) immunolabeling of the nodose ganglion (NG) of metabolically
706 challenged $Na_v1.8$-Cre-ChR2-YFP mice. **A, C, E**: CART-positive perikarya (AlexaFluor 594) across the
707 feeding groups. **B, D, F**: CART staining and endogenous ChR2-YFP fluorescence delineate the outline of
708 the vagal afferents. Asterisks are positioned over representative CART-positive cells. Note that CART
709 immunoreactivity is almost always contained within the cell membrane of the YFP-labeled cells, with a
710 few rare exceptions (arrowhead). Following visual inspection, the CART distribution pattern and intensity
711 appeared comparable across the feeding groups. Scale bars = 20 μm in A; applies to all images.

712 **Figure 7.** Estimates of CART-positive neurons and afferents across the feeding groups. **A**: The
713 percentage of YFP- and CART-positive neurons in the nodose ganglion (NG) of the $Na_v1.8$-Cre-ChR2-
714 YFP mice was not influenced by feeding status (n=7-8 per group). **B**: The percentage of CART-positive
715 varicosities in the area postrema (AP) was identical in the $Na_v1.8$-Cre-ChR2-YFP mice under different
716 feeding conditions. The data are expressed as the average of the means percentage ± maximum values
717 (n=7-8 per group). Each circle represents one value from one mouse. **C**: Frequency of CART
718 immunoreactivity profiles with varying intensity across feeding groups (n=7 per group). On the left,
719 frequency scattergraph of distributions of individual CART-positive cell profiles with median and
720 interquartile range. Each grey dot is one cell profile. The total number of profiles examined in each group
721 is annotated. On the right, the same data were represented as stacked bars after categorizations of
722 immunoreactivity level. Data are provided as means percentage ± SEM. **D**: Frequency of cells expressing
723 pCART mRNA in the nodose ganglia of fed (n=4) and fasted (n=3) wild-type mice. Cells were scaled
724 based on the intensity of hybridization signals. The total number of profiles examined in each group is
725 annotated. Stacked bars provide means percentage ± SEM.

726 **Figure 8.** (**A, B**): CART (55-102)-positive neurons in the nodose ganglia of lean Zucker rats.
727 Several digital images were stitched together (epifluorescence with Apotome filter). Many CART-
728 positive neurons (AlexaFluor 594) were observed in the nodose ganglion of fed and fasted rats. White
729 arrows indicate examples of CART neurons. Scale bar = 100 μm in A and applies to B.

730 **Figure 9.** CART (55-102) immunolabeling of the dorsovagal complex of metabolically
731 challenged $Na_v1.8$-Cre-ChR2-YFP mice. **A, B, C**: CART-positive (AlexaFluor 594) perikarya and fibers
732 of various origins were observed throughout the nucleus of the solitary tract (NTS) and area postrema
733 (AP). We noticed a trend toward increased immunoreactivity in the fasted groups. However, our estimates
734 (see Figure 6) indicate that the levels of CART in vagal afferents remained unchanged across feeding
735 conditions. **D, E, F**: CART immunoreactivity combined with endogenous ChR2-YFP fluorescence. **G**:
736 CART was very abundant in the AP. In particular, many YFP-labeled varicosities of vagal origin were
737 enriched for CART. However, we also observed CART immunoreactivity that was not contained in
738 ChR2-YFP-labeled fibers. **H**: High magnification of the distribution of CART immunoreactivity in the
739 vagal fibers of the AP in a single optical plan. Of note, CART frequently labeled the cytoplasm contained
740 within the YFP-labeled varicosities, which are indicated by arrowheads. Abbreviations: AP, area
741 postrema; NTS, nucleus of the solitary tract. Scale bars = 60 μm in A and applies to B-F; 15 μm in G; 5
742 μm in H.

Figure 10. Detection of prepro-CART (pCART) and prepro-MCH (pMCH) mRNAs using chromogenic ISH. **A**: pCART hybridization signals (brown DAB; brighfield optics) were strong in select hypothalamic nuclei. **B**: Throughout the nodose ganglion of fed mice, pCART signals of varying intensity were observed in many cell profiles. **C**: The nodose ganglion of fasted mice also contained pCART hybridization signals. **D:** Details of the hybridization signal in the nodose ganglion of one fasted mouse. Please note representative cell profiles without signal (*), or with low (l), medium (m), and high (h) signals. **E**: Hybridization signals for pMCH were very strong in neurons of the lateral hypothalamus. **F, G**: In contrast to the hypothalamus, pMCH signals were not observed in the nodose ganglia of fed and fasted mice. **H**: Details of the nodose ganglion of one fasted mouse showing several neuronal profiles completely devoid of signals (*). Tissue was counterstained with hematoxylin. Abbreviations: 3V, third ventricle; Arc, arcuate nucleus; DMH, dorsomedial hypothalamus; LHA, lateral hypothalamus; NG, nodose ganglion; VMH, ventromedial hypothalamus; ZI, zona incerta. Scale bars = 500 μm in A and E; 50 μm in B, C, F, G; 20 μm in D, H.

Figure 11. Absence of MCH staining in the vagal afferents of metabolically challenged $Na_v1.8$-Cre-ChR2-YFP mice. **A**: An antiserum against prepro-MCH (pMCH) labeled perikarya (AlexaFluor 594) in the lateral hypothalamus (LHA). **B**: PMCH was undetectable in the nodose ganglion (NG) of fasted $Na_v1.8$-Cre-ChR2-YFP mice. **C, D**: An antiserum against the MCH peptide labeled very few axons (arrowhead) in the medial NTS (SolM). MCH immunoreactivity was never observed in the YFP-labeled fibers of vagal origin. The arrowheads point to one MCH-positive axon. AP, area postrema; NTS, nucleus of the solitary tract; sol, solitary tract. Scale bars = 40 μm in A and B; 10 μm in C.

Figure 12. CART (55-102) immunolabeling of peripheral ChR2-YFP-labeled fibers. **A**: ChR2-YFP fibers contained within the cervical vagus nerve. CART was not detected in the vagus nerve. We obtained similar results in the cervical and subdiaphragmatic nerves on both sides. **B**: In whole mounts of the gastric muscularis, numerous GFP-positive axons and specialized endings can be observed. The leafy structure may correspond to an intraganglionic laminar ending (arrowhead) of vagal origin. CART immunoreactivity was abundant in large varicose fibers and, to a lesser extent, the cell body of enteric neurons (EN). Nonetheless, CART immunoreactivity was not found in GFP-stained fibers. Abbreviations: IGLE, intraganglionic laminar ending; EN, enteric neuron. Scale bar = 10 μm in A and B.

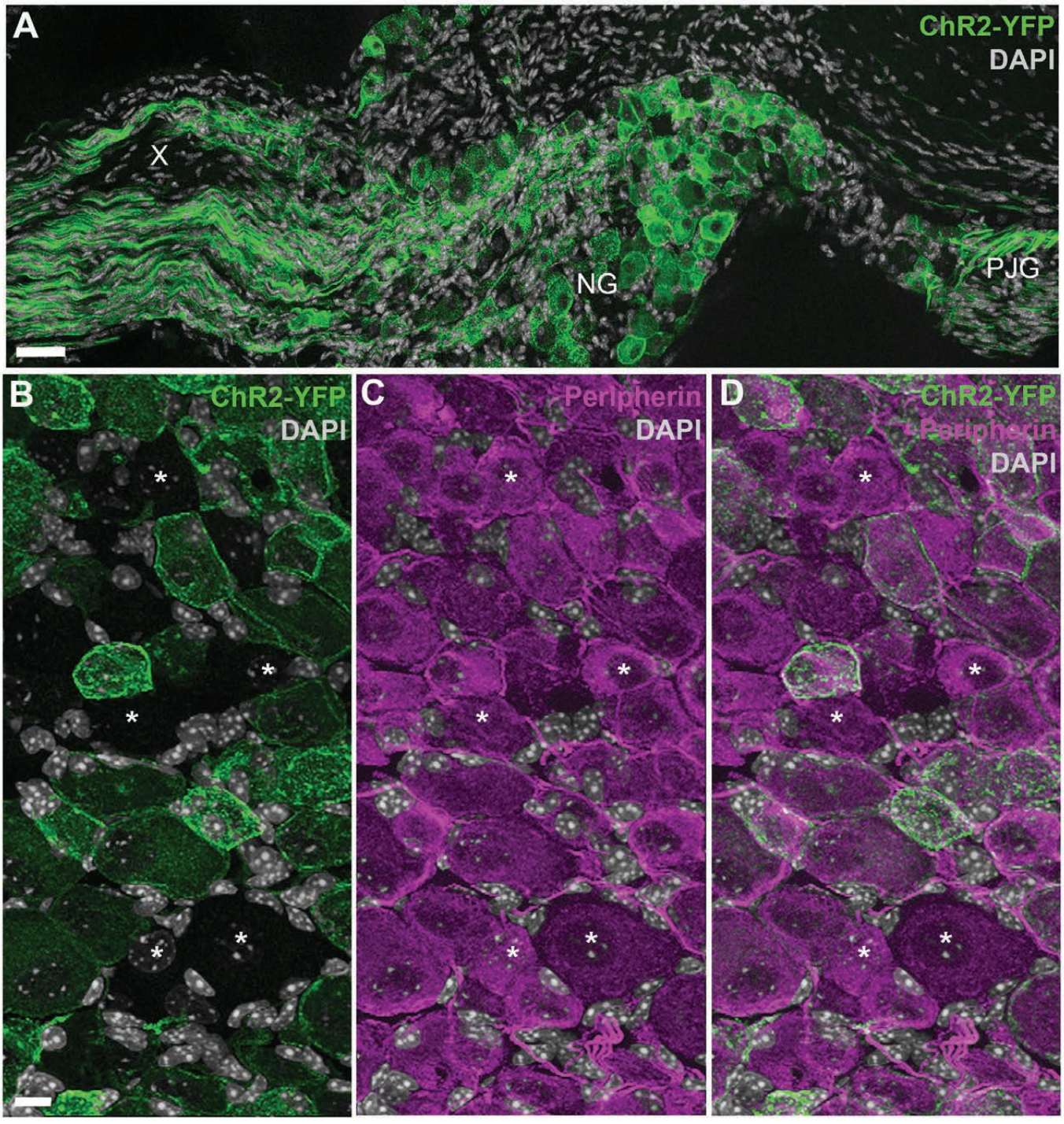

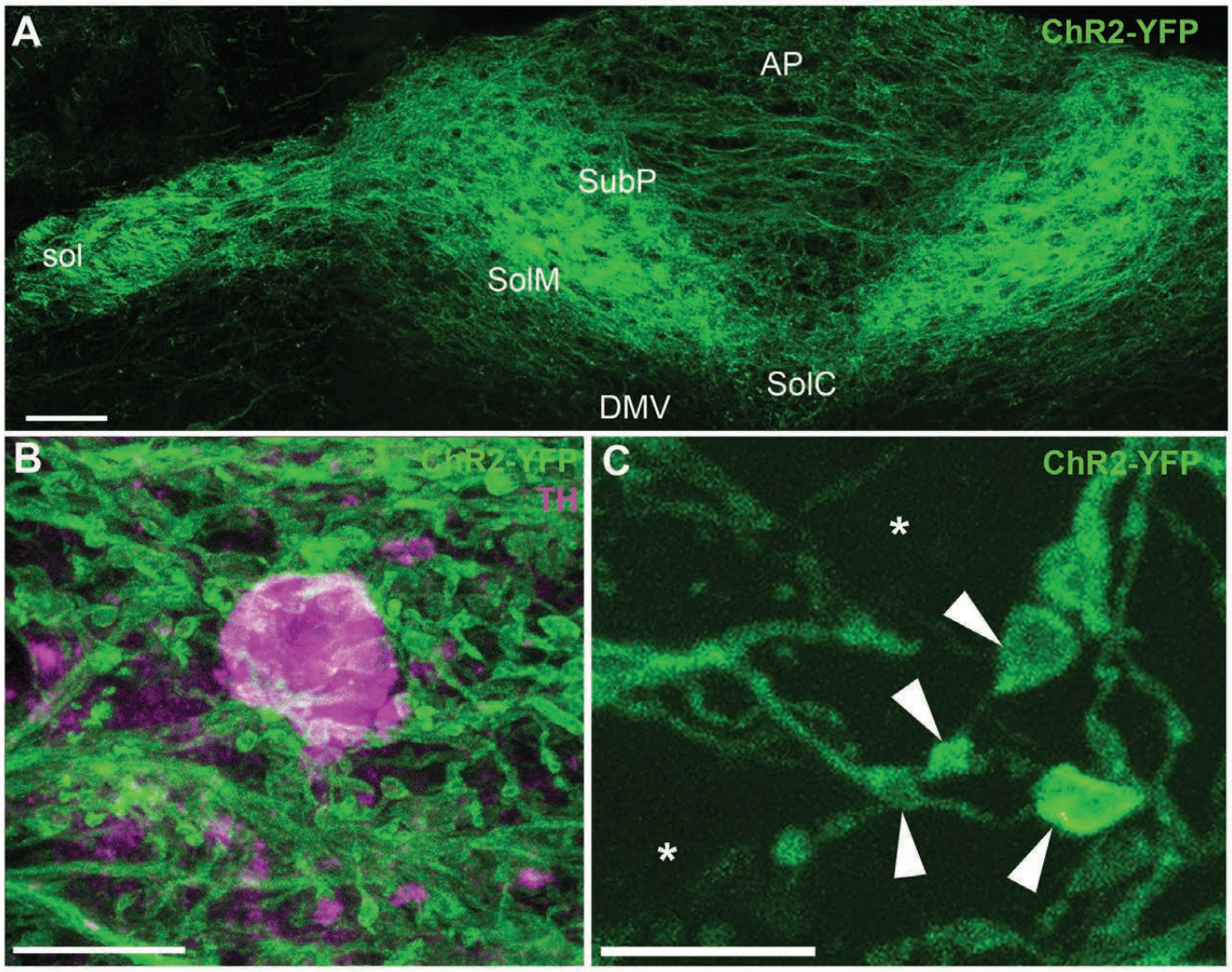

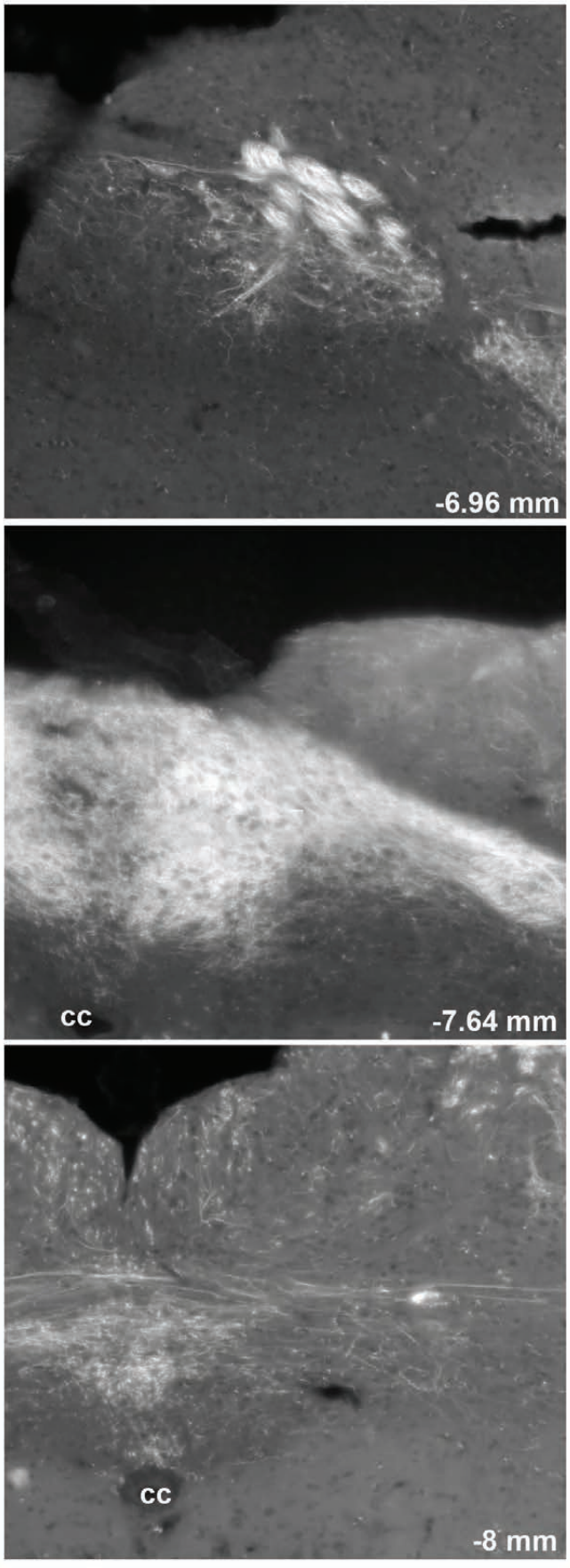

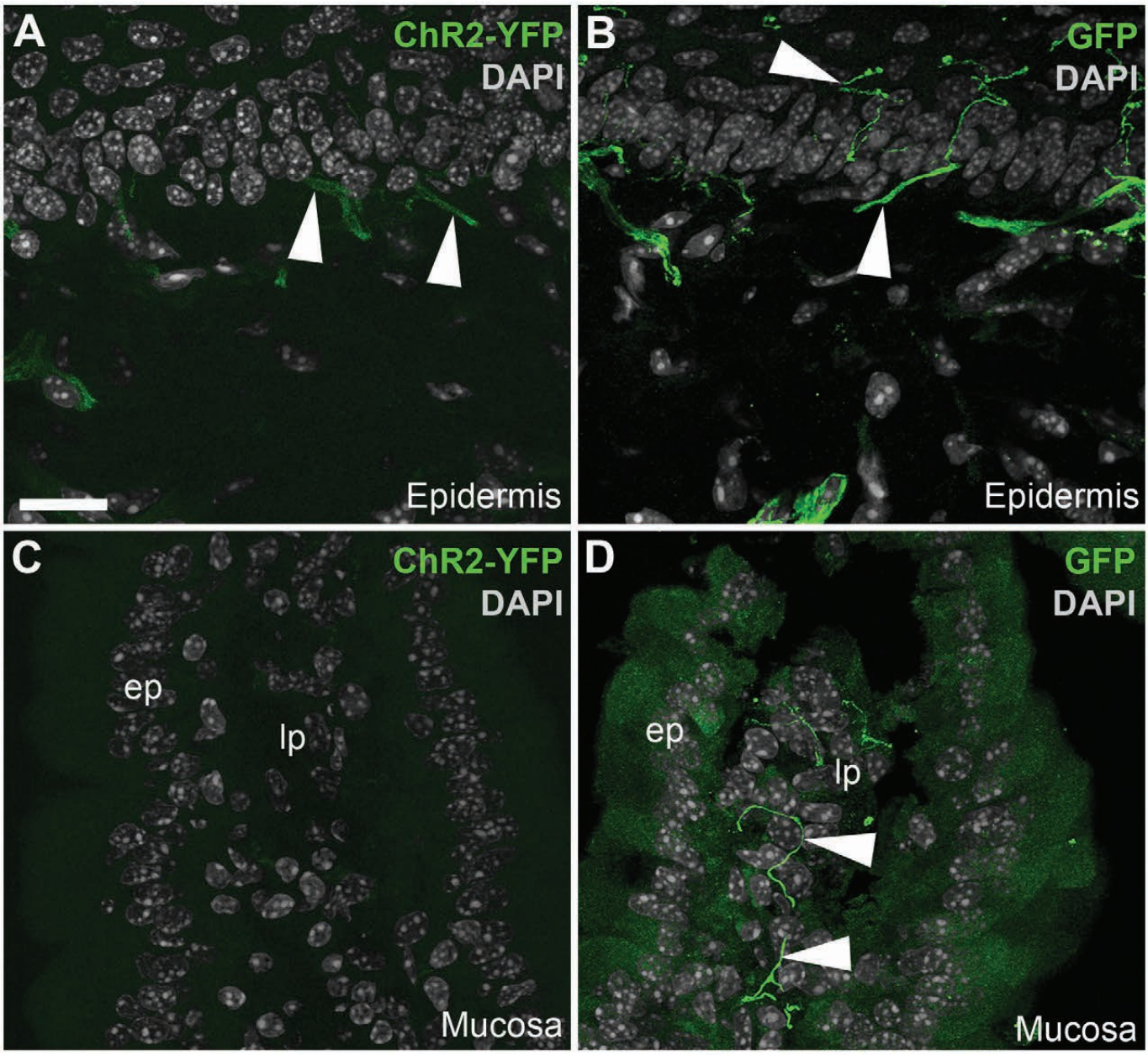

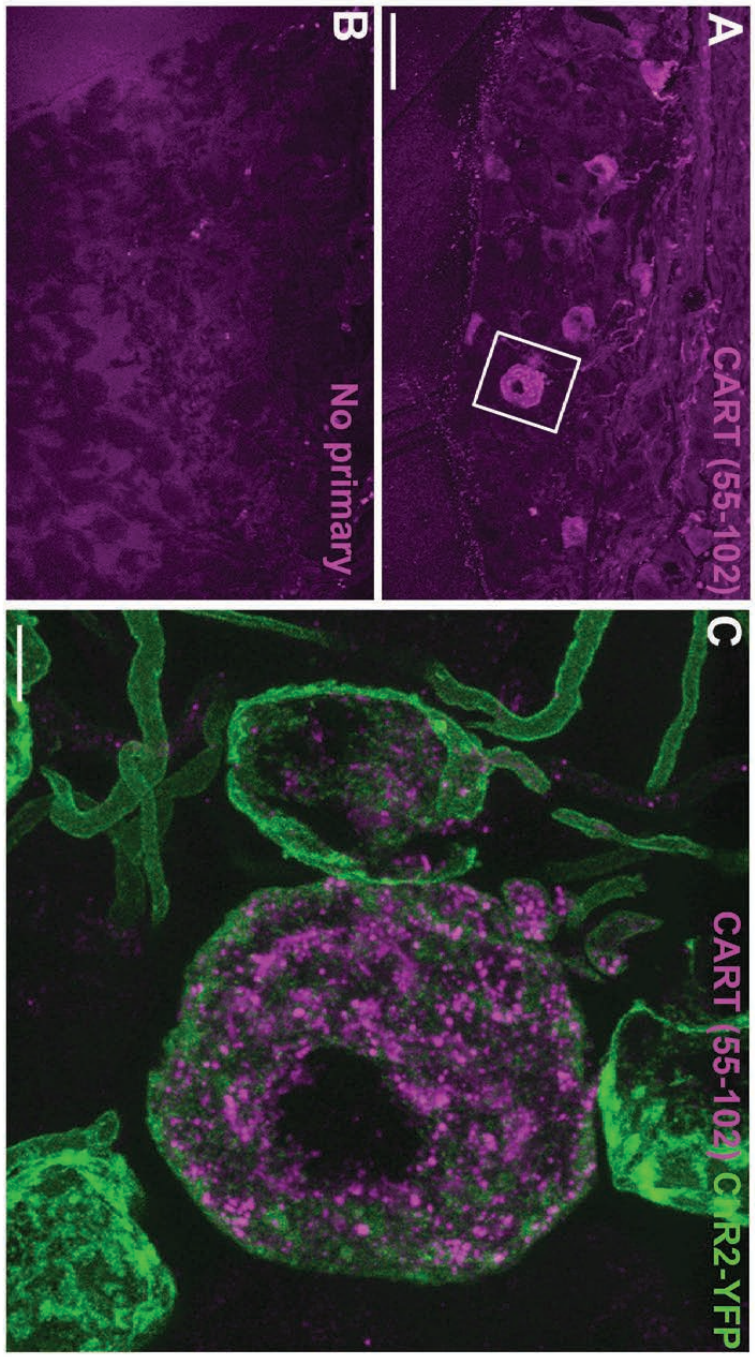

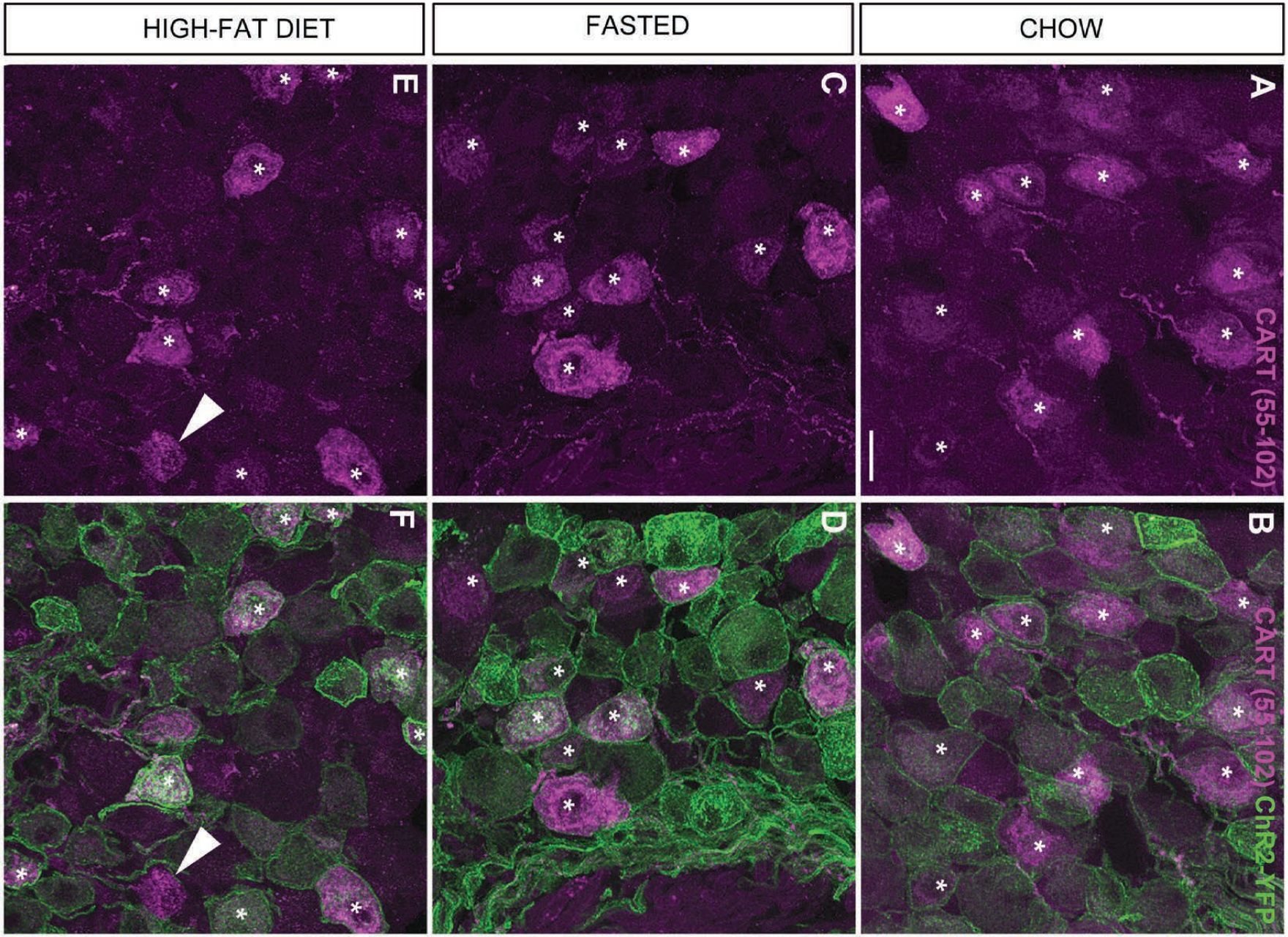

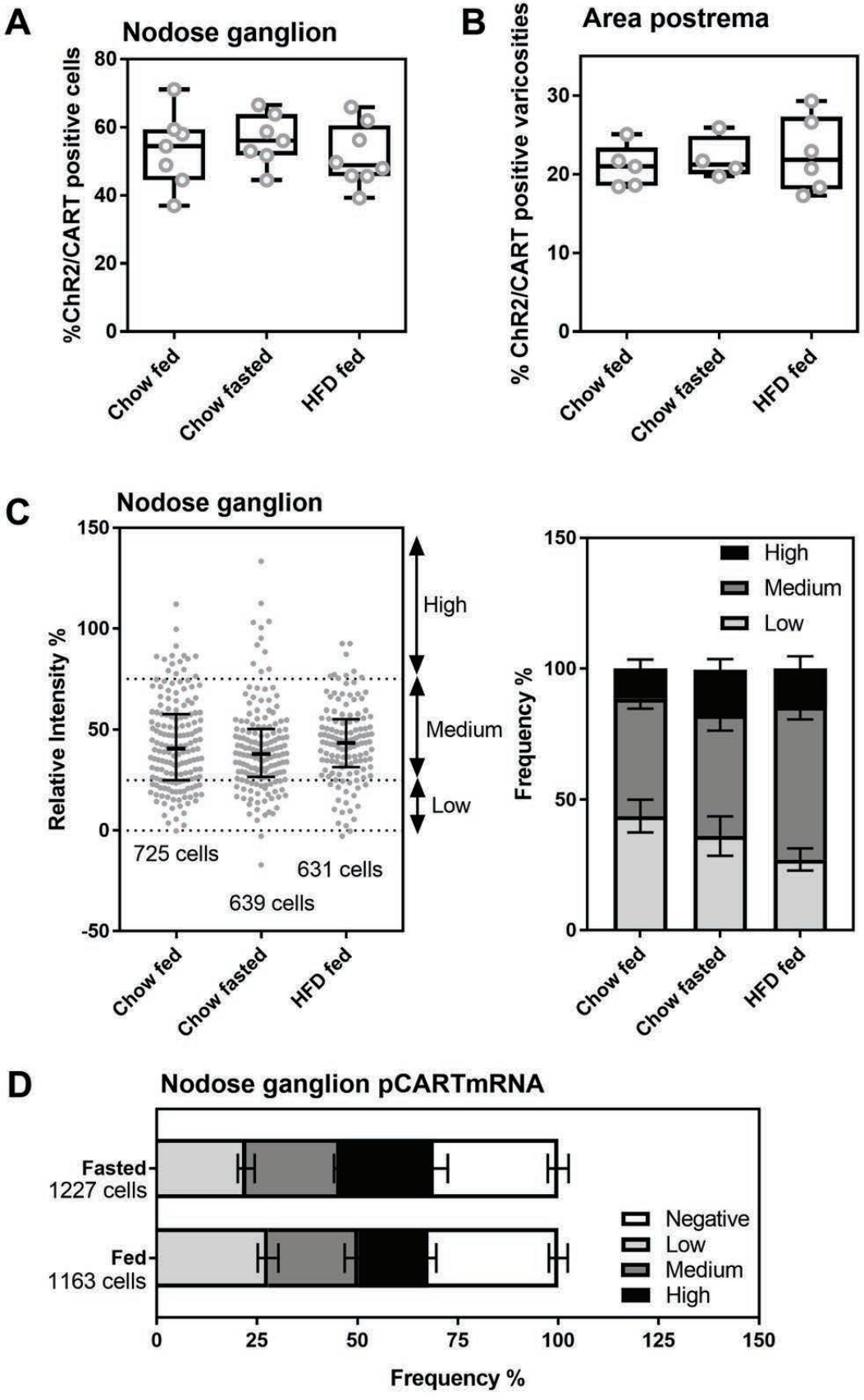

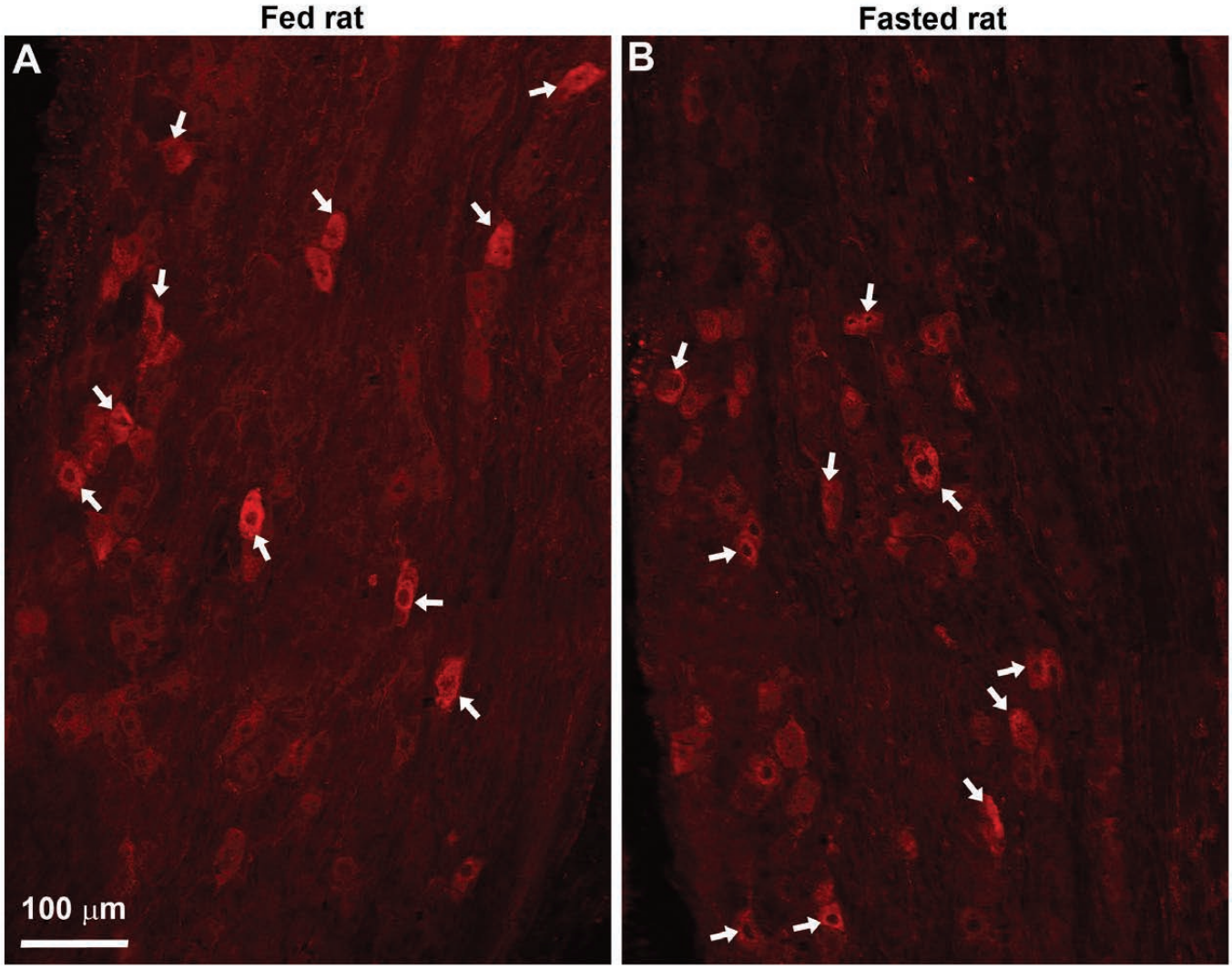

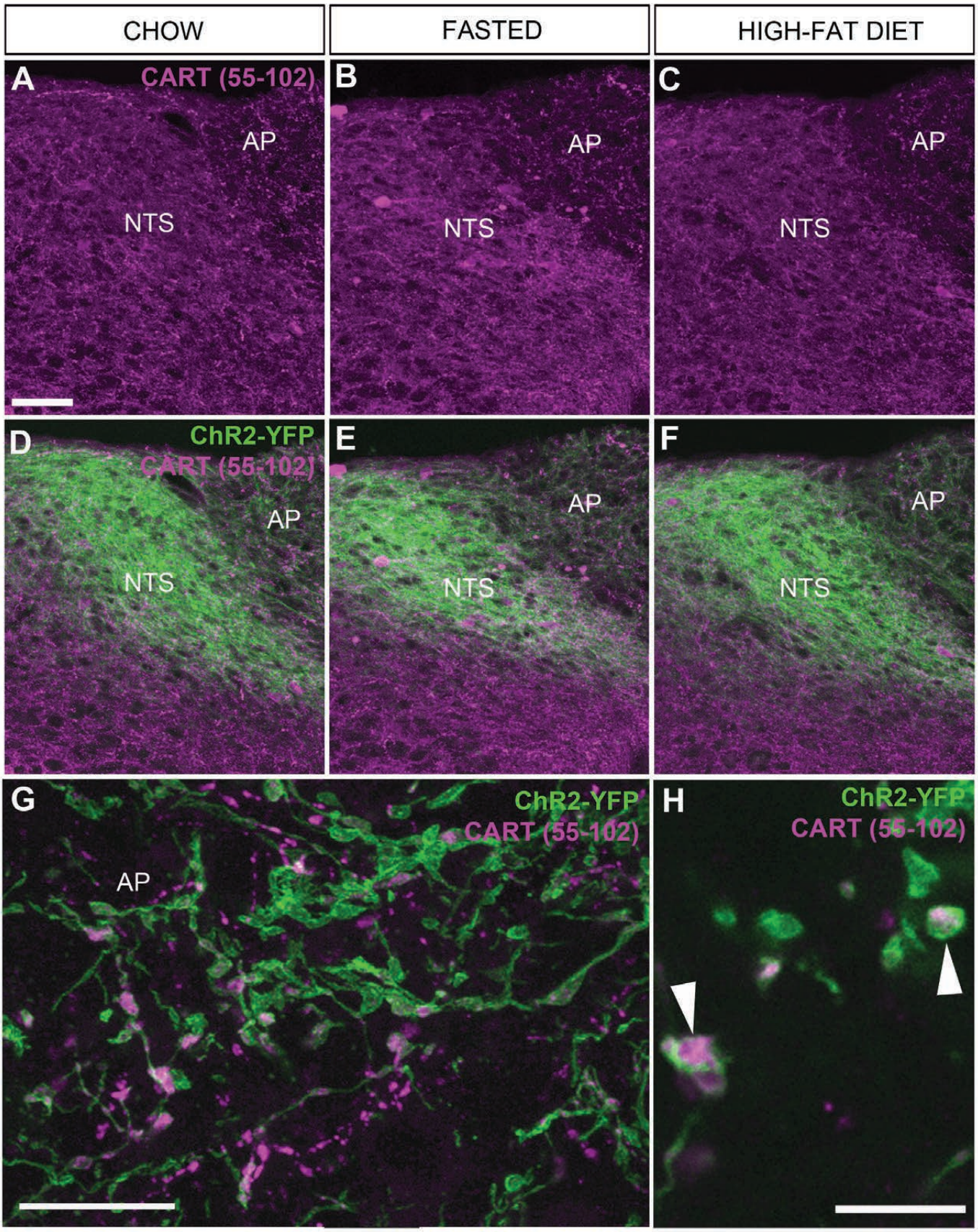

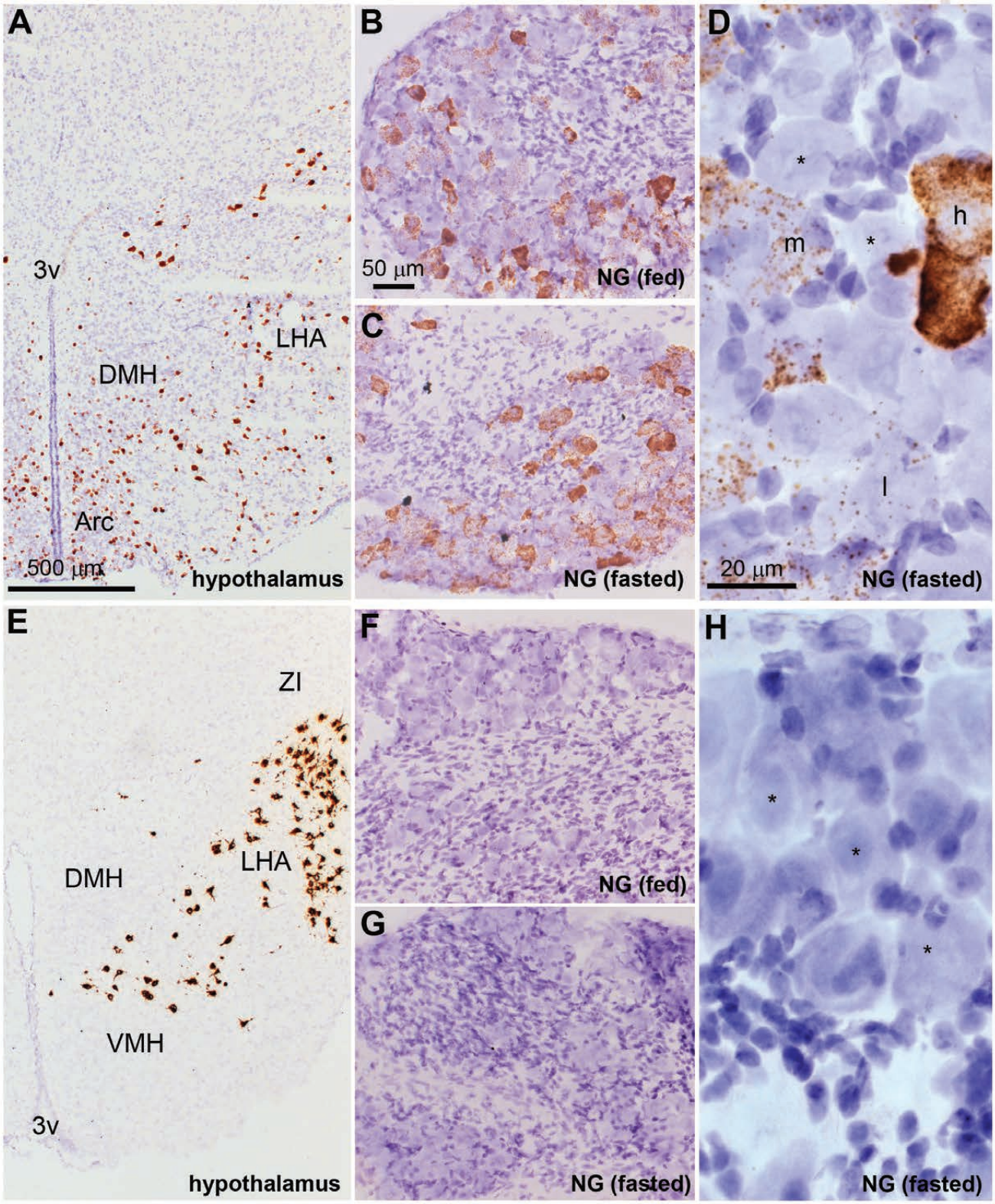

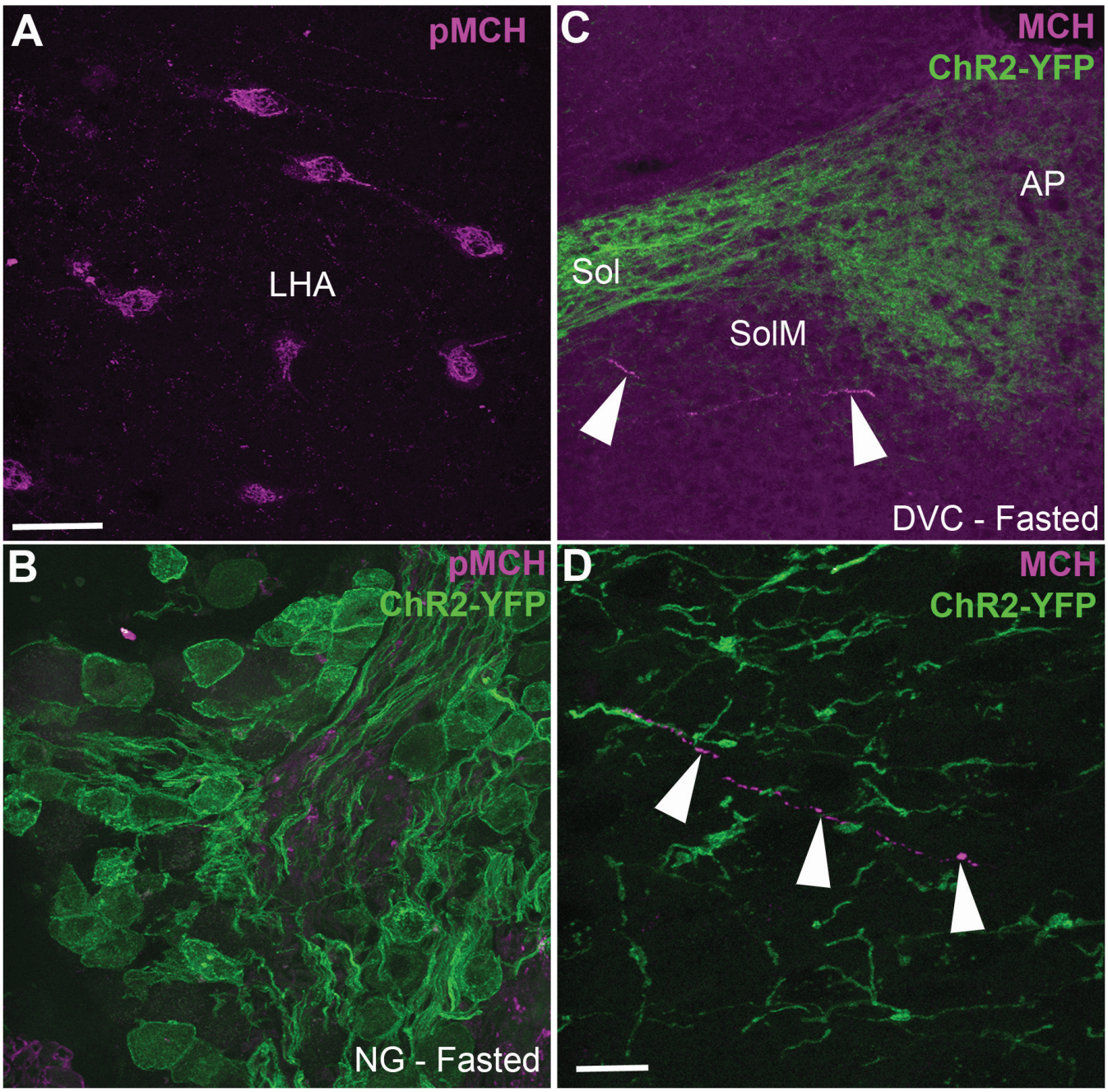

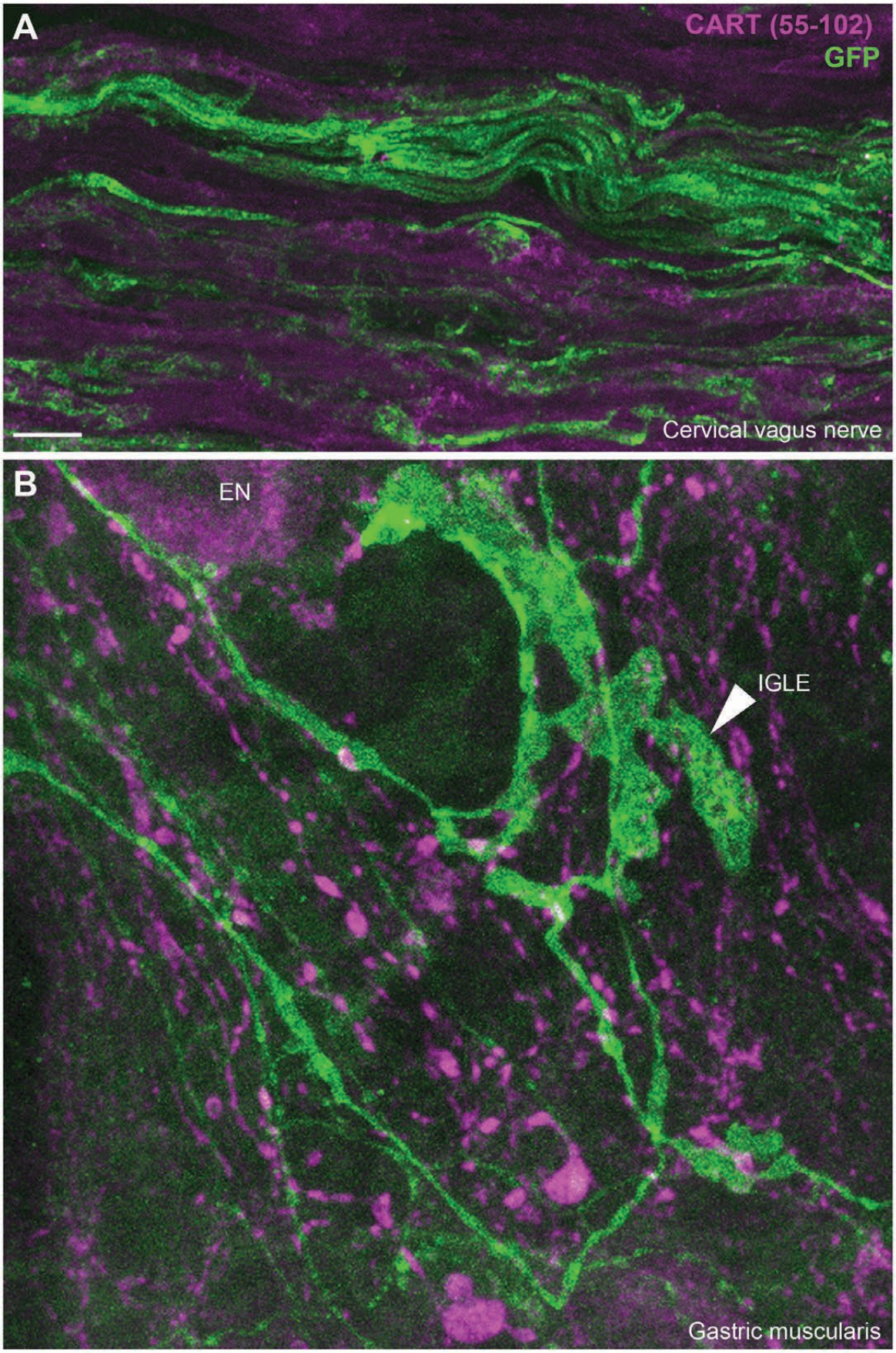

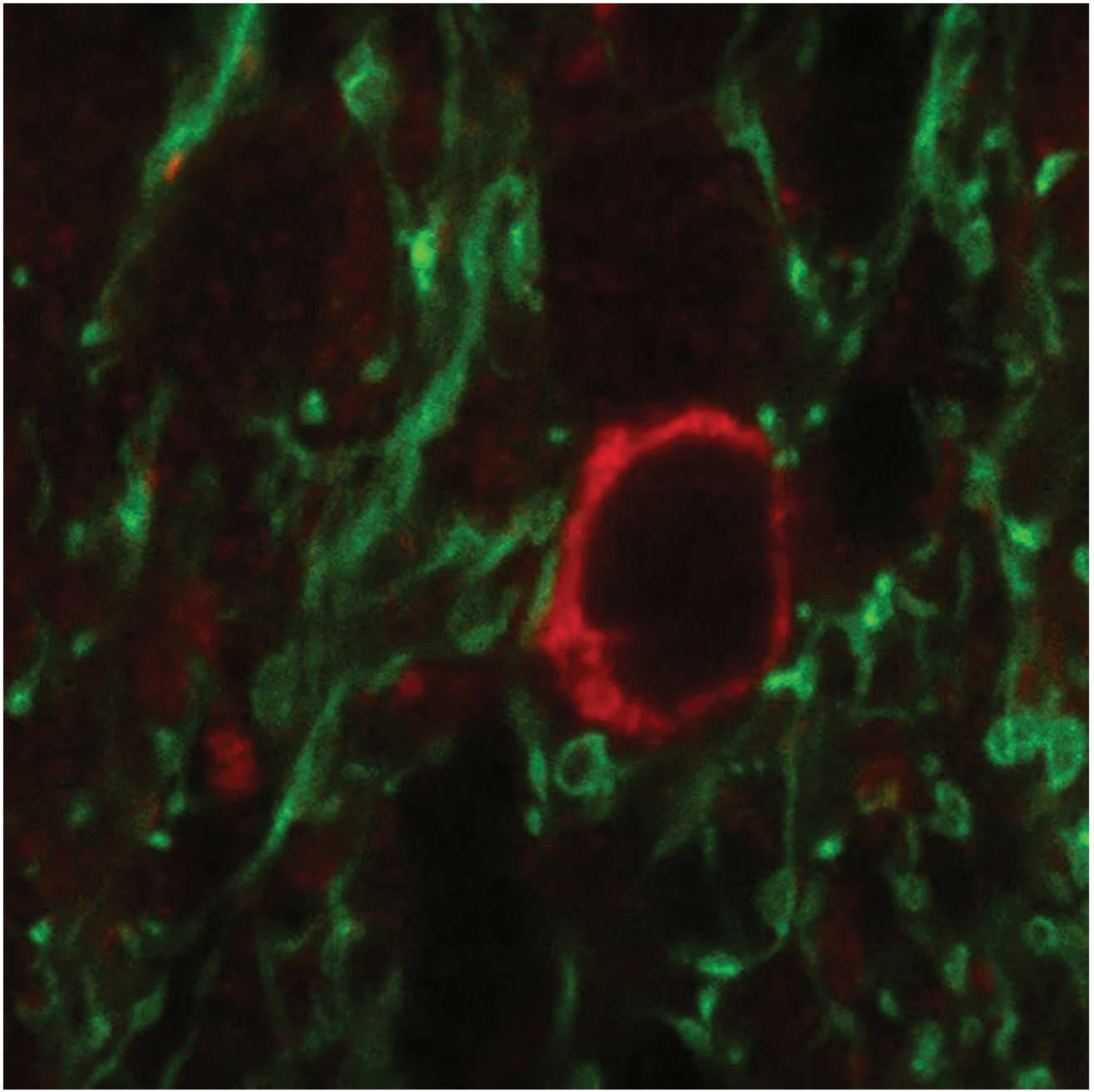

Primary antibody	Manufacturer	Cat#	Lot#	Host	Working dilution	Immunogen
Peripherin	EMD Millipore	AB1530	2446692	Rabbit	1:500	trp-E-peripherin fusion protein containing all but the 4 N terminal amino acids of rat peripherin
CART 55-102	Phoenix pharmaceuticals	H-003-62	01251-10; 01251-6		1/800 – 1/1,000	Ile-Pro-Ile-Tyr-Glu-Lys-Lys-Tyr -Gly-Gln-Val-Pro-Met-Cys-Asp -Ala-Gly-Glu-Gln-Cys-Ala-Val-Arg-Lys-Gly-Ala-Arg-Ile-Gly-Lys-Leu-Cys -Asp-Cys-Pro-Arg-Gly-Thr-Ser -Cys-Asn-Ser-Phe-Leu-Leu-Lys-Cys-Leu [Disulfide bonds between Cys1-Cys3,Cys2-Cys5,Cys4-Cys6]
CART 1-39		H-003-63	01102			pGlu - Glu - Asp - Ala - Glu - Leu - Gln - Pro - Arg - Ala - Leu - Asp - Ile - Tyr - Ser - Ala - Val - Asp - Asp - Ala - Ser - His - Glu - Lys - Glu - Leu - Pro - Arg - Arg - Gln - Leu - Arg - Ala - Pro - Gly - Ala - Val - Leu - Gln
MCH		H-070-47	01629-3		1/1,000	Asp-Phe-Asp-Met-Leu-Arg-Cys-Met-Leu-Gly-Arg-Val-Tyr-Arg-Pro-Cys-Trp- Gln-Val
TH	Abcam	ab101853	GR120879-17	Goat		Synthetic peptide corresponding to human TH 30-100 (N terminal)
ProMCH	Santa Cruz Biotech.	sc-14509	B2415		1/100 – 1/1,000	20-amino-acid peptide near the C-terminus of pro-MCH precursor of human origin
GFP	Aves Lab	GFP-10120	GFP697986	Chicken	1/1,000	GFP emulsified in Freund's adjuvant
Secondary antibody	**Manufacturer**	**Cat#**	**Lot#**	**Host**		
Anti-Rabbit AlexaFluor5	Life	A21207	1256153	Donkey		

94	Technologies			
Anti-Goat AlexaFluor594		A11058	1608643	
Anti-Chicken AlexaFluor488		A11039	1356650	Goat

Table 1. Information relative to the primary and secondary antisera used in the study.

Table 2. List of reagents used for *in situ* hybridization.

ISH RNAScope probes from ACD				
Gene name(s)	**Accession #**	**Target region**	**Cat#-channel**	**Chromogenic labels**
CARTPT	NM_013732.7	11 - 860	432001-c1	DAB - brown
PMCH	NM_029971.2	4 - 652	478721-c1	DAB - brown